CZECH TECHNICAL UNIVERSITY IN PRAGUE

FACULTY OF ELECTRICAL ENGINEERING

Doctoral Thesis

August 2008   Ing. Martin Vejmelka

CZECH TECHNICAL UNIVERSITY IN PRAGUE

FACULTY OF ELECTRICAL ENGINEERING

DEPARTMENT OF CYBERNETICS

QUANTIFYING INTERACTIONS BETWEEN COMPLEX OSCILLATORY SYSTEMS: A TOPIC IN TIME SERIES ANALYSIS

Doctoral Thesis

Ing. Martin Vejmelka

Supervisor: RNDr. Milan Paluš, DrSc.

Acknowledgments

Abstract

This work is focused on the problem of identifying interactions between complex dynamical oscillatory processes. Discovering relationships in complex systems plays an important role in the process of understanding how subsystems cooperate to create complicated behavior. There are two main problems in interaction analysis: directionality analysis and synchronization detection. Synchronization is a process of mutual alignment of rhythms of two systems indicating a stronger form of cooperation. Directionality analysis is concerned with asymmetric interactions between systems and facilitates the discovery of drive-response relationships. Current frameworks for detecting synchronization and directionality are recounted, their properties are analyzed and new approaches to both problems are proposed. An experimental dataset is analyzed with the goal of describing changes in the human cardiorespiratory system between the waking state and general anesthesia. The proposed methods can be used in the context of nonlinear dynamics to investigate coupled biological, geological, meteorological, chemical and other types of process.

Abstrakt

Tato práce se zaměřuje na problém hledání interakcí mezi komplexními oscilačními procesy. Nalezení vnitřních souvislostí mezi jednotlivými procesy je důležitým krokem k hlubšímu pochopení funkce složitých systémů. Zde se soustředíme na dva hlavní problémy analýzy párů dynamických procesů: určení směru působení a testování synchronizace. Cílem analýzy směru působení je odhalení řídících vztahů mezi procesy. Zjištění synchronizace, sladění rytmů dynamických procesů, ukazuje na užší součinnost dvou procesů. Jsou popsány současné metody zpracování časových řad, které slouží k vyšetřování těchto jevů. Pomocí detailních numerických experimentů jsou analyzovány vlastnosti vybraných metod a jsou předloženy nové možnosti řešení obou problémů. Závěrem práce je zpracována předběžná studie experimentálně získaných dat, která porovnává interakce v lidském kardiorespiračním systému v klidu při vědomí a během celkové anestézie. Navržené metody lze využít v rámci aplikace teorie nelineární dynamiky k analýze vzájemného ovlivňování biologických, meteorologických, chemických a dalších systémů

Contents

List of Figures

Chapter 1

Introduction

Recently, new approaches to understanding the behavior of complex systems based on results of non-linear dynamics have come to the forefront of current research. This tendency is becoming clearer as more and more problems from geology, meteorology, physical, chemical and life sciences have been more satisfactorily understood after reformulating them in the framework of non-linear dynamics. Especially in biological and life sciences, important components of physiological systems, such as the human body, have been modeled as a set of coupled non-linear dynamical oscillators: the heart, the brain and the lungs. When trying to understand complex systems, scientific advances depend on developments in theoretical and experimental science and on building links between hypothesized models and experimental results.

The present work "Quantifying interactions between complex oscillatory systems: a topic in time series analysis" is focused on building links between theoretical and practical aspects of complex systems modeling. The goal of the work is the analysis, comparison and further development of selected time series analysis algorithms aimed at uncovering interactions between coupled oscillatory systems with a minimum of assumptions on the form of the interactions.

This study is organized as follows: the Introduction continues with a basic treatment of important concepts in non-linear dynamics and types of interactions, Chapter 2 describes current methods of quantification of direc-

tionality, Chapter 3 introduces some methods for quantifying dependencies between time series, Chapter 4 introduces the concept of significance testing. Chapter 5 describes the original developments in the problem of detecting directional influence and in the problem of detecting synchronized states. Chapter 6 contains detailed numerical studies of the performance of the methods. In Chapter 7 selected methods are applied to real data obtained during in the course of a study of changes occurring in the human cardiorespiratory system when under general anesthesia. Chapter 8 contains a discussion of the results and describes planned further work.

1.1   Self-sustained non-linear oscillators

There are several assumptions about the investigated systems that are required by the subsequent theoretical analysis. In particular, it is assumed that the systems are *self-sustained non-linear oscillators.* A self-sustained oscillator is a dissipative dynamical system which generates oscillatory motion using energy obtained from an internal source. The characteristics of the (quasi)oscillatory motion depend exclusively on the structure and parameters of the system: one can thus think of the system as producing a natural rhythmic activity. Linear oscillatory systems do not exhibit stable limit cycles and their final trajectory depends on the initial conditions under which the system was set into motion. Non-linear systems on the other hand may have a non-trivial attractor region, such as a limit cycle. A majority of real physical systems are necessarily dissipative, especially so in life sciences, and if stable motion along a given trajectory is to be followed, an energy source must be available to supply the energy lost in each cycle. The non-linearity serves to establish a stable intensity of oscillation [2]. Some systems that have bee investigated in the framework of the above constraints are the human heart [3], the brain [4, 5], weather systems [6, 7] and geological activity [7]. Alternatively the framework can be applied to systems the motion of which is constrained to a strange attractor. This is characteristic of systems exhibiting complex behavior known as deterministic chaos.

In Fig. 1.1 the limit cycle of the well known Van der Pol oscillator is
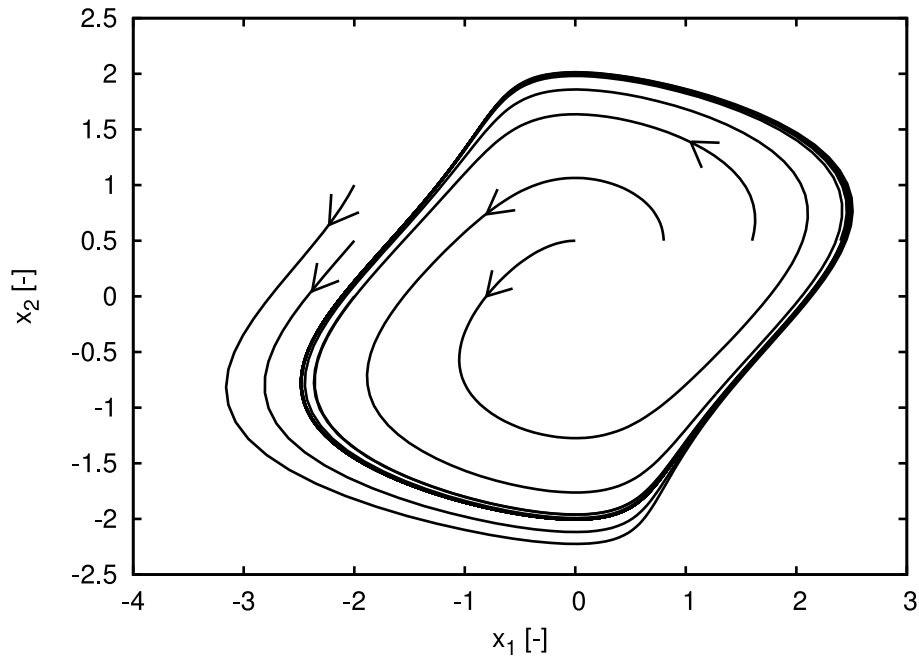
Figure 1.1: The limit cycle of the Van der Pol oscillator. The plot shows the points $(x_1, x_2) = (x, \dot{x})$ resulting from integrating the equation (1.1) with $\mu = 0.2$.

shown as an example of a nonlinear dynamical system exhibiting a stable limit cycle. The Van der Pol system is given by the differential equation

$$\ddot{x} - \mu(1 - x^2)\dot{x} + \omega^2 x = 0, \tag{1.1}$$

where ω controls the frequency of the Van der Pol system and μ controls the shape of the limit cycle (for $\mu = 0$ the system is an undamped harmonic oscillator).

1.2 Amplitude and phase

The motion of systems satisfying the criteria laid out in the above paragraph can be decomposed into two primary variables: amplitude and *phase*. The amplitude of the limit cycle represents the intensity of the oscillations and is stable as seen in Fig. 1.1, where the trajectories starting from points outside

of the limit cycle return to it after a transient period. Phase represents the position of the system along the limit cycle and is free: it is neither stable nor unstable. Phase is an observable of the system that characterizes its motion along the attractor (in the direction of the zero Lyapunov exponent). Phase is required to be a monotonic function of time and it must grow by a fixed amount (usually 2π) when a cycle is completed. Phase grows without bound but values of phase which differ by a multiple of 2π represent the same physical state.

If the motion of the system is perturbed by a weak external force, the variations in amplitude decay in time and the system returns to the limit cycle. However if the perturbation also shifted the system in the direction of the limit cycle, changing its phase, then that change of phase is preserved. Phase can thus be affected by very weak forces. The supposition that the forces acting on the system are weak is important to ensure that the motion of the system can be decomposed into an independent amplitude and phase and that the system does not qualitatively change its behavior [2].

1.3   Time series analysis

A time series is a record of the values of an observable at a sequence of time instants. A time series is different from a general set of data because a total ordering by time is imposed on the samples. Also, in the case of dynamical systems successive samples tend to be highly correlated unless the system is undersampled. In the following, it is always assumed that a pair of time series measured at the same time from both systems is available as a source of information about their activity. I has been previously shown [8, 9, 10] that under some conditions, it is possible to recover the topology of the attractor from a univariate time series measured from a dynamical system using the technique of *time-delay embedding*. A univariate time series thus contains a wealth of information about the behavior of the underlying deterministic processes.

A univariate time series exhibiting oscillatory behavior may be used to obtain a phase time series describing the motion of the dynamical system

along its attractor. Many different methods can be applied to extract a phase signal but not all methods are suitable for all situations. One of the approaches involves finding a two-dimensional projection of the attractor set that rotates around a fixed point. This point is then selected as a center of rotation and the angle from the horizontal axis to the line connecting the center of rotation with the instantaneous position of the system on the projection defines the phase. A two-dimensional projection can be obtained by either using a time-delay embedding [8, 9], using difference coordinates or by finding a general projection formula.
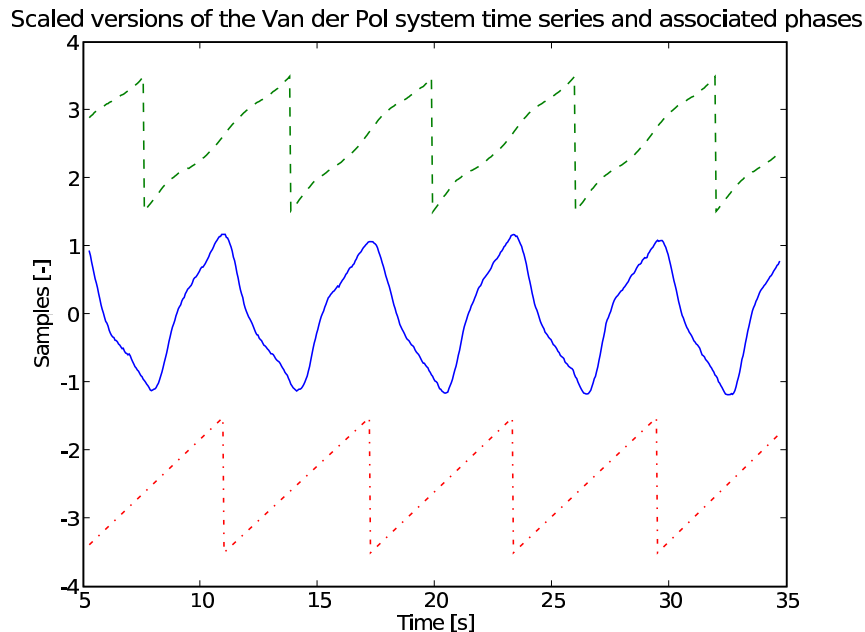
Figure 1.2: Time series obtained from the Van der Pol oscillator (solid line), phase extracted using the Hilbert transform (dashed line) and phase extracted using the marked events method by detecting the peaks (dash-dot line). Signals have been rescaled and shifted vertically for presentation purposes.

More commonly used approaches are based on the analytical signal concept [11]. In these methods, the imaginary part of the original real signal is constructed. The time series then consists of complex values having a unique amplitude and phase, which is then simply taken as the phase of the

oscillation. There are two main frequently used methods of obtaining the imaginary part: the Hilbert transform and the wavelet transform. Reference [12] has shown that in many circumstances the methods give similar results. It is recommended that the source time series is bandpass filtered to create a narrow-band series if there is no clear oscillation frequency. This approach is however not without its dangers as narrow band filtering might attenuate or partially obscure the activity of a process the main frequency of which exhibits substantial fluctuations. The Hilbert transform has been applied to broadband EEG signals (e.g. [13]) but the physical meaning of the phase time series computed in this way is unclear [12].

An example is shown in Fig. 1.2 where phase was extracted from the time series of the Van der Pol system by computing the imaginary part of the signal using the Hilbert transform. Phase acts as an indicator of the evolution and history of the system. When the phase signal conforms to the standard definition above it is sometimes termed "unwrapped" phase. At times it is advantageous to subtract 2π from the phase signal upon the completion of each cycle. The resulting signal thus has range $[0, 2\pi)$ and and there is a one-to-one mapping between phases and physical states. This is sometimes termed "wrapped" phase as the transformation corresponds to "wrapping" the phase signal around a unit circle. The phase signal in Fig. 1.2 follows the definition of a "wrapped phase". This is useful when trying to estimate the probability density function of the phase time series. The problem setting can be understood by reviewing the schema in Fig. 1.3.

An alternate technique for extracting so called marked-events phase is to find an event that occurs once in every cycle of the investigated system at a fixed time. A good example is the occurrence of the R-peak of the electrocardiogram (ECG) signal. In the time interval between two successive events the phase must (by definition) increase by 2π. The phase is interpolated linearly between the two events. This technique is useful if the signal is difficult to treat with other methods (this is the case of the ECG signal) or excessively noisy but with well-identifiable events.
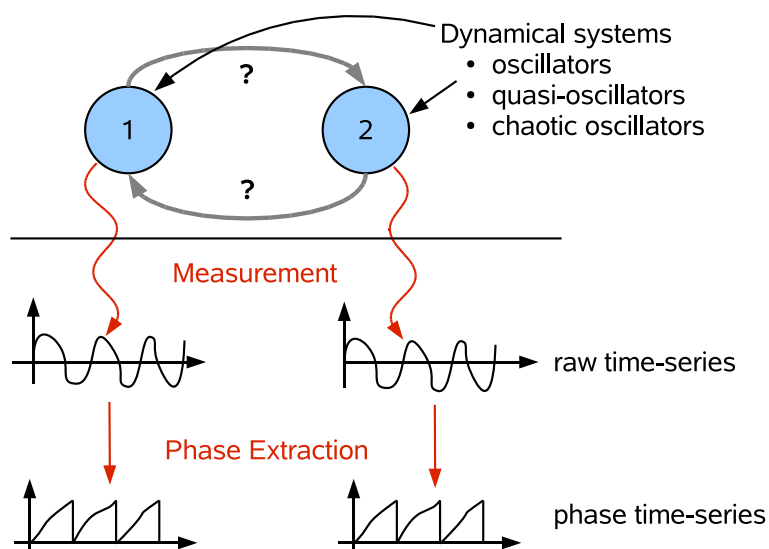
Figure 1.3: Schematic depiction of the process of observing possibly coupled systems, measuring time series and obtaining a phase.

1.4 Weak interactions

Weak interactions between systems are interactions that do not qualitatively affect the behavior of either coupled system. It is in general difficult to precisely discriminate between weak and strong coupling. A coupling that is too strong binds the systems together so that their behavior is no longer decomposable into two separate processes. The investigated coupling should not be so strong as to deprive the systems of their individuality [2].

When investigating how two systems interact together, two main questions arise. The first question concerns the strength of the coupling: if the coupling is strong enough it causes the two systems to *synchronize*, or mutually align their rhythms. Multiple forms of synchronization have been discovered since the first known description of identical synchronization in pendulum clocks by Christiaan Huygens in 1673 [14]. If the coupling is weak enough so that the systems do not yet synchronize, it is possible to investigate the *directionality of coupling*, in other words the asymmetric properties of the coupling.

1.4.1   Directionality analysis

An important problem arising from the analysis of coupled systems is the detection of directionality of coupling. In general when analyzing only two systems, four distinct situations can arise: the systems are uncoupled, they are unidirectionally coupled (two possibilities) or they are bidirectionally coupled. Directionality analysis can also be applied to systems that have dissimilar dynamics, where coupling strength is an ill-defined notion [15]. Analysis of directionality is an important problem as it reveals drive-response relationships in complex systems composed of multiple subsystems.

Asymmetric interactions have been studied for example in the human cardio-respiratory system [16] or in EEG signals [17]. However directionality analysis in non-linear oscillatory processes is a relatively new discipline and methods of analysis must be sufficiently evolved before they can be confidently applied to experimental data. There are many competing approaches and problem formulations that must be thoroughly investigated and compared on model problems so that their properties are understood.

One of the main problems facing an experimenter today is the apparent lack of standardized testing procedures. These "testing protocols" would allow one to compare the multitude of methods of quantifying interactions between systems. It is common practice that newly proposed methods are tested on a very simple model system and then directly applied to a complex experimental problem which is obviously much more difficult than the model system. In this work, adequate testing of methods is highly emphasized before applying them to experimental data.

1.4.2   Synchronization

The second problem on which this work focuses is the detection of synchronized states. Synchronization has recently attracted considerable interest from theoreticians as well as experimentalists (e.g. the monograph [2]), since synchronization and related phenomena have been observed in systems studied not only in physics, but also in natural and social sciences, medicine and technology. Examples include cardio-respiratory interaction [3, 18, 19], syn-

chronization of neural signals [20, 21, 22, 23] or episodes of synchronization between meteorological variables reflecting interactions in the climate system [6, 7].

The strongest definition of synchronization requires that the difference between states of synchronized systems asymptotically vanishes. This definition is called *identical synchronization* [24], while the notion of *generalized synchronization* requires that states of coupled systems are (asymptotically) related by some function [25, 26]. Even weak couplings can result in *phase synchronization*, which relates the instantaneous phases of the systems, while their amplitudes can be uncorrelated [1].

1.5   Example model systems

In this section, some frequently used model systems are introduced and their typical behavior and phase extraction mechanisms are described.

1.5.1   Lorenz system

The Lorenz system is a three-dimensional deterministic dynamical system named after its constructor Edward Lorenz in 1963 [27] and is a heavily simplified model of the convection rolls in the atmosphere. The model was shown to exhibit a sensitive dependence on initial conditions. The equations of two coupled Lorenz systems with coupling in the x variable are shown below

$$
\begin{aligned}
\dot{x}_{1,2} &= \sigma(y_{1,2} - x_{1,2}) + \epsilon_{1,2}(x_{2,1} - x_{1,2}) \\
\dot{y}_{1,2} &= x(\rho - z_{1,2}) - y_{1,2} \\
\dot{z}_{1,2} &= xy - bz,
\end{aligned}
\tag{1.2}
$$

with σ being the Prandtl number and ρ the Rayleigh number. The parameters $\epsilon_{1,2}$ represent the strength of coupling from one system to the other and are not part of the original model. The system exhibits chaotic behavior for $\rho = 28$ but has periodic orbits for other values of this parameter

Since the system is able to generate chaotic behavior, it's dimension must be greater than 2 and is less than or equal to 3 as that is the number of

differential equations. The Hausdorff dimension of the (strange) attractor of this model was estimated by Grassberger and Procaccia [28] in 1983 to be 2.06 ± 0.01.
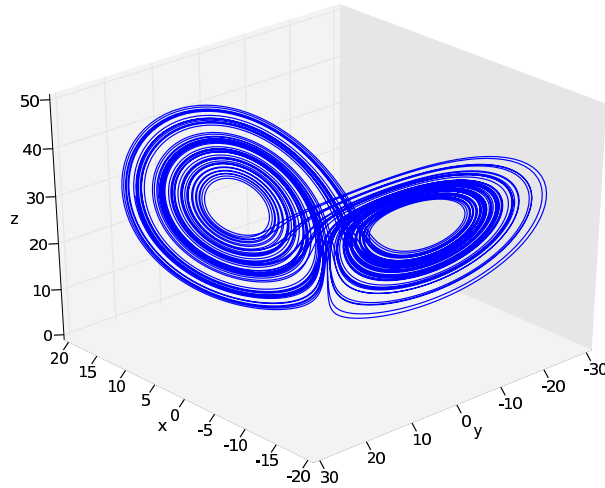
Figure 1.4: The Lorenz attractor ($\rho = 28$, $\sigma = 10$ and $b = 8/3$). Integrated using Runge-Kutta 4th order scheme with dt = 0.005, 16384 points shown.

The trajectory of the Lorenz system in the phase space is very well-known and has the shape of a butterfly (cf. Fig. 1.4).

1.5.2 Rössler system

Another paradigmatic system exhibiting chaotic behavior is the Rössler oscillator which was proposed by Otto Rössler [29] and grew out of his thinking about the Lorenz attractor. Later the equations have been found to model some types of chemical reactions. The equations characterizing two coupled Rössler oscillators are given as:

$$
\begin{aligned}
\dot{x}_{1,2} &= -\omega_{1,2}y_{1,2} - z_{1,2} + \epsilon_{1,2}(x_{2,1} - x_{1,2}) \\
\dot{y}_{1,2} &= \omega_{1,2}x_{1,2} + a_{1,2}y_{1,2} \\
\dot{z}_{1,2} &= b_{1,2} + z_{1,2}(x_{1,2} - c_{1,2}),
\end{aligned}
\tag{1.3}
$$

The correlation dimension of the Rössler attractor ($a = 0.15$, $b = 0.2$, $c = 5.7$) is ≈ 2.014 [30]. The Rössler attractor has a characteristic shape

which is shown on Fig. 1.5. As is usual for chaotic oscillators the behavior of
the system is very sensitive to the parameters used. The parameters of the
Rössler system can be adjusted so that the system rotates around a center in
the x-y plane and phase can then be simply extracted. For some parameter
settings however, the Rössler system has a "funnel" attractor where no such
center around which the motion proceeds can be found. In this case, other
ways of extracting phase such as the method of Osipov *et al.* [31] must be
used. These methods allow the extraction of phase from curves (trajectories)
with positive curvature.
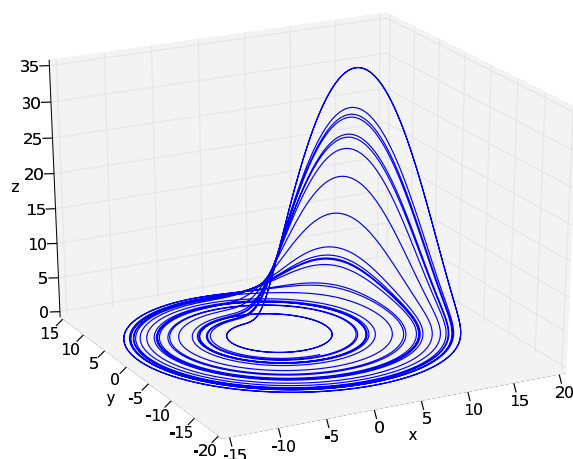
Figure 1.5: The Rössler attractor ($a_{1,2} = 0.15$, $b_{1,2} = 2$, $c_{1,2} = 10$). Integrated
using the Runge-Kutta 4th order scheme with dt=0.01, 16384 points shown.

Chapter 2

Quantifying directional influence

Quantifying asymmetric properties of the coupling between systems from time series is a problem that involves making several assumptions about the investigated system pair. In the analysis framework, it is assumed that interdependencies in the time series arise from coupling between the two systems. Most importantly it is assumed that there is no third system driving both of the analyzed systems, possibly with different delays. If there is knowledge of such a third system and its time series can be obtained, it is sometimes possible to eliminate its influence on the system pair under scrutiny, however this is difficult at present and the issue becomes much more difficult if the systems are different in dynamics.

The first step in detecting directional influence is developing an index which reacts to the strength of directional coupling. The introduction of several such indices will be the subject of this Chapter. However it is important to note that such an index does not as of itself constitute a complete method of detecting coupling directionality. When processing experimental data the situation is quite complicated. Measurement noise and limited length of experimental time series can be sources of considerable additional variance in the estimates. Different statistical and dynamical properties (stochasticity, dominant frequencies) of the two underlying systems can cause severe bias

in estimates of directionality indices. We show how it is possible to alleviate these effects to a large extent by testing the computed indices using sets of *surrogate data* [32, 33].

2.1 Approaches to quantifying directionality

At present there are three main approaches to detecting directionality in bivariate time series. The first approach is based on state-space reconstruction or mutual prediction, the second approach is based on modeling functional relationships of phases and the third approach involves estimating information-theoretic functionals.

State space methods include various cross-prediction methods and methods based on statistics of nearest neighbors. Cross-prediction methods attempt to directly exploit Granger's ideas on mutual forecasting of series generated by coupled linear systems [34]. Generally the attractor in state space is reconstructed by means of a time-delay embedding [35, 8, 9]. However opposite opinions exist on how to interpret the cross prediction accuracy, e.g. in Ref. [20] the authors hypothesize that the average cross-prediction error is smaller in the driving system while in [21] it is suggested that the cross-prediction error should be smaller when predicting the driven system. Alternative methods exploit statistics based on nearest neighbor distances [36], however in Ref. [37] the authors assert that other factors such as the effective dimension at typical neighborhood sizes may influence the result of the previously published algorithms.

The second group involves estimating functional relationships between phases of the systems. In Ref. [38] the authors try to estimate the Fourier coefficients of the coupling function and subsequently compute a norm based on a subset of the coefficients indicating the directionality. However this approach was found to be accurate only for long time series [15]. The method has been improved with a bias correcting term and an estimate of significance of the directionality by Smirnov and Bezruchko [39].

The last group of methods consists of algorithms based on information theory. Here, Schreiber [40] proposes to compute the *transfer entropy*, based

on the Kullback-Leibler entropy measuring the deviation of the transition probability density function (PDF) from the generalized Markov property. Paluš [41] has applied information theoretic functionals to phases to detect "net flow of information" between processes. This approach will be detailed in the following section. Recently it has been shown that the method of Schreiber can be identified with the method of Paluš for a certain set of parameters [42].

2.2 Information theoretic approaches

Quantities based on information theoretic functionals have enjoyed an important position in detecting relationships between complex systems partly due to their non-parametric nature which makes them widely applicable. The presented method involves estimating a well-known information theoretic functional — the conditional mutual information (CMI) [43]. There is a multitude of ways to estimate the CMI [42]. Some of the estimation methods are presented here and their characteristics are described.

Consider discrete random variables X and Y with sets of values Ξ and Υ respectively and probability distribution functions (PDFs) $p(x)$, $p(y)$ and the joint PDF $p(x, y)$. The *Shannon entropy* $H(X)$ is defined as

$$H(X) = -\sum_{x \in \Xi} p(x) \log p(x), \tag{2.1}$$

The *joint entropy* $H(X, Y)$ of X and Y is

$$H(X, Y) = -\sum_{x \in \Xi} \sum_{y \in \Upsilon} p(x, y) \log p(x, y) \tag{2.2}$$

for discrete sets Ξ, Υ. It is straightforward to extend the definition to more than two variables. *Conditional entropy* $H(Y|X)$ of Y given X is

$$H(Y|X) = -\sum_{x \in \Xi} \sum_{y \in \Upsilon} p(x, y) \log p(y|x).$$

The average amount of common information contained in the variables X and Y is quantified by the *mutual information* $I(X;Y)$ defined as

$$I(X;Y) = H(X) + H(Y) - H(X,Y). \qquad (2.3)$$

The *conditional mutual information* $I(X;Y|Z)$ of the variables X, Y given the variable Z is given as

$$
\begin{aligned}
I(X;Y|Z) &= H(X|Z) + H(Y|Z) - H(X,Y|Z), & (2.4)\\
&= I(X;Y;Z) - I(X;Z) - I(Y;Z), & (2.5)\\
&= H(X,Z) + H(Y,Z) - H(Z) - H(X,Y,Z), &
\end{aligned}
$$
$$(2.6)$$

all of which are theoretically equivalent. However, depending on the method used to compute entropy or mutual information, some of the above formulae will be more appropriate than others in particular situations. Entropy and mutual information are measured in *bits* if the base of the logarithms in their definitions is 2. In this work the natural logarithm is used and therefore the estimates are given in *nats* unless the unit is explicitly indicated.

A generalized version of the Granger causality concept [34] is that if the time series generated by one process provides us with information on the time series generated by another process at some point in the future, the first process influences the second process. If only two processes are involved and coupling is detected exclusively in one direction it is inferred that the first process causally influences the second process. Granger has applied his principle to coupled linear models [34]. In Ref. [44] it has been demonstrated that using changes in cross-prediction errors to indicate the directionality of coupling is not trivially extensible to non-linear systems. On the other hand methods based on information theory have been shown to be widely applicable, especially when the estimators of the relevant information theoretic functionals are non-parametric and thus independent of the form of the probability density distribution (usually under some mild technical assumptions).

Let X and Y denote two stationary ergodic processes and $x(t)$, $y(t)$ their time-series. The presented method of detecting coupling directionality uses conditional mutual information as an indicator of the presence of net information flow [41] between the two analyzed systems characterized by their respective time series. The net information flow $I(X; \Delta_\tau Y | Y)$, where $\Delta_\tau Y$ is an observable derived from the state of the process Y in the future (τ denotes the time difference), is defined as the mutual information between X, Y and $\Delta_\tau Y$ that is not a result of the action of the history of process Y on itself, i.e. excluding $I(Y; \Delta_\tau Y)$ and is also not the result of common history of the two processes captured by $I(X; Y)$. A statistically significant information flow thus indicates that information is being transferred between the process X and the process Y at some later point in time. This can be readily interpreted as an influence of the process X on the process Y in the future. The detection criterion is based on two indices

$$i_{X \to Y} = \frac{1}{N} \sum_{\tau=1}^{N} I\Big(x(t); \Delta_\tau y(t) \Big| y(t)\Big), \qquad (2.7)$$

$$i_{Y \to X} = \frac{1}{N} \sum_{\tau=1}^{N} I\Big(y(t); \Delta_\tau x(t) \Big| x(t)\Big), \qquad (2.8)$$

where the notation

$$I\Big(x(t); \Delta_\tau y(t) \Big| y(t)\Big)$$

denotes mutual information between $x(t)$ and $\Delta_\tau y(t)$ conditioned on $y(t)$. The operator Δ_τ represents for example the difference

$$\Delta_\tau x(t) = x(t + \tau) - x(t).$$

The series $x(t), y(t)$ can contain the values generated by the respective systems or values which have been derived from the original time series. In general, each of the time-series $x(t), y(t)$ should be considered multivalued. This is the case if state space reconstruction techniques [8] are applied prior

to computing the information theoretic functionals [44].

In the following sections different types of estimators of entropy or mutual information will be thoroughly investigated.

2.2.1 Binning methods

Binning methods are frequently applied to estimating information-theoretic functionals. Binning methods discretize the space of the signal samples into bins or boxes inside which the probability density function (PDF) is assumed to be constant. Binning methods thus estimate a coarse profile of the PDF over the entire sample space.

Classical methods involve histogram binning, also referred to as equidistant binning. This estimator of multidimensional entropy of time series and its bias has been investigated by Moddemeijer [45], who derived the necessary bias correction terms. Fraser and Swinney [46] have proposed an adaptive spatial subdivision scheme for automatically estimating the optimal partition for computing mutual information. Darbellay *et al.* [47, 48, 49] have improved on this scheme by supplying a stopping condition of the subdivision scheme. The stopping condition is based on Dobrushin's information theorem [50].

Pompe has proposed computing generalized mutual information (based on Rényi's second order entropy [51]) from ranked time series [52]. Computing statistics from ranked time series has the advantage of being invariant with respect to smooth transformations of coordinates.

Paluš [18, 23, 41, 7, 44] has used equiquantal binning, where each time series is partitioned so that there is an approximately equal amount of samples in each bin. The width of each bin thus adjusts to the density of samples in each region — dense regions contain small bins and sparse regions contain large bins. Additionally, an estimator constructed in this way can be viewed as the estimator that maximizes all marginal entropies during the estimation (keeping all parameter values fixed).

Recent efforts include a an estimator of entropy based on B-splines [53] by Daub *et al.* [54]. The algorithm however runs in $O(NM^3)$ time, which

is exceptionally slow for a binning algorithm. Here N denotes the number of points in a time series and M the number of bins. Estimation of multidimensional entropies constitutes sufficient means to indirectly compute mutual information with (2.3) and also the conditional mutual information using (2.6). In classical binning approaches to computing mutual information, data points close to bin boundaries can cross over to a neighboring bin due to noise or fluctuations, thus introducing additional variance into the computed estimate. To overcome this problem, Daub *et al.* have proposed a generalized binning method, which makes use of B-Spline functions to assign data points to bins. The sample space is divided into equally sized bins as in equidistant binning. A major difference between classical binning and generalized binning is that in generalized binning, a data point is assigned to multiple bins simultaneously with weights given by (implicitly normalized) B-Spline functions. The shape of the B-Spline functions is determined by their order k, which is a parameter of the method. With B-Spline order 1, each point is assigned to exactly one bin and the method is equivalent to simple equidistant binning. The proposed method is thus a fixed binning scheme extended with a preprocessing step designed to reduce the variance.

A B-Spline function is defined with the help of a knot vector

$$t_i = \begin{cases} 0 & i < k \\ i - k + 1 & k \le i \le M - 1 \\ M - 1 - k + 2 & i > M - 1 \end{cases} ,$$

where M is the total number of bins and i is an index into the knot vector. B-spline functions are defined (and evaluated) recursively [53] by

$$B_{i,1}(z) = \begin{cases} 1 & t_i < z < t_{i+1} \\ 0 & \text{otherwise} \end{cases} ,$$

$$B_{i,k}(z) = B_{i,k-1}(z) \frac{z - t_i}{t_{i+k-1} - t_i} + B_{i+1,k-1} \frac{t_{i+k} - z}{t_{i+k} - t_{i+1}}.$$

The standard definition of computing entropy (2.1) is used with

$$p(x_i) = \frac{1}{N} \sum_{j=1}^{N} B_{i,k}(f_{M,k}(x_j)), \tag{2.9}$$

where $f_{M,k}(x)$ is a linear transformation which maps the values of x onto the domain of the B-Spline functions [54]. In two dimensions it is necessary to compute the joint PDF [54]

$$p(x_i, y_j) = \frac{1}{N} \sum_{l=1}^{N} B_{i,k}(f_x(x_l)) \times B_{j,k}(f_y(y_l)). \tag{2.10}$$

This procedure can be readily generalized to three dimensions

$$p(x_i, y_j, z_l) = \frac{1}{N} \sum_{m=1}^{N} B_{i,k}(f_x(x_m)) \times \\ \times B_{j,k}(f_y(y_m)) \times B_{l,k}(f_z(z_m)). \tag{2.11}$$

The computation of $I(X;Y|Z)$ can thus be written as

$$I_{M,k}(X;Y|Z) = H_{M,k}(X,Z)+ \\ +H_{M,k}(Y,Z) - H_{M,k}(Z) - H_{M,k}(X,Y,Z),$$

and each of the terms may be computed using the formulae (2.9), (2.10) and (2.11) together with (2.1) and (2.2). The notation $I_{M,k}(X;Y|Z)$ and $H_{M,k}(X,Y)$ indicates that the method has two parameters M — the number of bins and k — the order of the B-Spline. For further analysis, the order of the B-Splines is fixed at $k = 3$ as this was order employed in Ref. [54].

2.2.2 Metric methods

Metric methods depend on the notion of distance in a space. These methods are sensitive to the distribution of samples and to the distribution of their distances. Metric methods generally compute a local approximation of density for each sample in the series and use these estimates to determine

the entropy of the set of samples. Alternatives are available where entropy is estimated directly from various sample statistics instead of estimating the probability density function (PDF) of the time series first.

There are two main possibilities in determining the approximate PDF in a region close to a given reference point. In the first method, a volume around the point is fixed (usually a hypersphere) and the number of points inside that volume is counted. The other possibility is to fix a number of points to find and search for the minimal bounding hypersphere which contains that number of points closest to the reference point. In both cases the value of the PDF is then approximated as a constant function inside this hypersphere: the number of points is divided by the volume to obtain a density estimate.

The term redundancy is frequently used as a synonym for multidimensional mutual information in the context of dynamical systems. Redundancies based on correlation integrals (CI) use a fixed volume approach to estimating the local PDF. The connection between the correlation integral and local probability densities is elucidated in [55]. The correlation integral has been introduced by Grassberger and Procaccia [28] in the context of estimating the correlation dimension of strange attractors. The correlation integral is given by

$$C(\mathbf{x}, \epsilon) = \frac{1}{N(N-1)} \sum_{i=1}^{N} \sum_{j=1, j \neq i}^{N} \Theta(\epsilon - ||x_i - x_j||),$$

where $||\cdot||$ represents the selected metric, $\Theta(\cdot)$ is the Heaviside function and ϵ is the radius of the hypersphere in which neighbors are sought. Savit $et\ al.$ [56] show how the conditional redundancy $R(x_1; x_m|x_2, ..., x_{m-1}, \epsilon)$ may be computed. The conditional redundancy quantifies the dependency between x_1 and x_m conditioned on $x_2, ...x_{m-1}$.

$$R(x_1; x_m|x_2, ..., x_{m-1}, \epsilon) =$$
$$= -\log \frac{C(x_1, ..., x_{m-1}, \epsilon)C(x_2, ..., x_m, \epsilon)}{C(x_1, ..., x_m, \epsilon)C(x_2, ..., x_{m-1}, \epsilon)},$$

Inspired by this approach, Prichard and Theiler [55] have extended the con-

cept of conditional redundancies to multiple variables and propose computing the time-lagged mutual information between two time series with

$$
\begin{aligned}
I(x; y, l, \epsilon) &= H(x(t), \epsilon) + H(y(t-l), \epsilon) \\
&- H(x(t), y(t-l), \epsilon)
\end{aligned}
$$

where the Shannon entropy $H(x, \epsilon) \approx -\log[C(x, \epsilon)]$. In this work, the conditional mutual information is estimated using the formula

$$
I(x; y_\tau | y, \tau, \epsilon) = I(x(t); \Delta_\tau y(t) | y(t), \epsilon) =
$$
$$
= -\log \frac{C(x(t), y(t), \epsilon) C(\Delta_\tau y(t), y(t), \epsilon)}{C(x(t), \Delta_\tau y(t), y(t), \epsilon) C(y(t), \epsilon)}.
$$

It has been shown that the estimate of the mutual information using correlation integrals converges if $\epsilon \to 0$ [55]. However in data sets of finite size, small sample effects are observed which disrupt the convergence behavior of the estimator.

2.2.3 Kernel methods

Kernel methods are more restrictive than metric methods and require not only distances to be defined but also a space in which samples are assigned coordinates. Due to the numerical nature of most time series this is not a stringent restriction. Mutual information from bivariate time series was first estimated using a kernel estimate of local density by Moon *et al.* [57]. According to Steuer *et al.* [58] this method was found to be superior to the classical histogram (binning) methods.

Kernel density estimator introduced by Silverman [59] in one dimensional space is defined as

$$
f(x) = \frac{1}{Nh} \sum_{i=1}^{N} K\left(\frac{x - x_i}{h}\right) \tag{2.12}
$$

where h is the kernel width parameter. The kernel function $K(x)$ is required to be a probability density function. It follows that also f itself is a probability density. The selection of h is crucial but most methods for selection

thereof are usually computationally intensive. Silverman suggests using h which minimizes the mean integrated square error, assuming the underlying distribution is Gaussian. Steuer *et al.* [58] objected against a straightforward introduction of a kernel density estimator into the logarithmic formula of mutual information. The discretization of the (x, y)-plane into infinitesimal bins corresponds to the continuous form of mutual information.

$$I(X, Y) = \iint_{(X,Y)} f(x, y) \log \frac{f(x, y)}{f(x)f(y)} dx dy. \qquad (2.13)$$

But such a correspondence does not hold for the individual entropies used in the formula $I(X, Y) = H(X) + H(Y) - H(X, Y)$ [42]. The discretization introduced by numerical integration for computing the above integral does not correspond to the partition of data. It has been shown [58] that the estimated mutual information is much less sensitive than the probability density itself.

2.3   Example results

In this section, the characteristics of a selection of the estimators are shown on a linear model, where the conditional mutual information functional can be computed analytically. The selected model is a pair of two unidirectionally coupled linear parts of the Barnes sunspot model [60]

$$
\begin{aligned}
z_i^{[1]} &= \alpha_1 z_{i-1}^{[1]} + \alpha_2 z_{i-2}^{[1]} + a_i^{[1]} - \beta_1 a_{i-1}^{[1]} - \beta_2 a_{i-2}^{[1]} \\
z_i^{[2]} &= \alpha_1 \left[\epsilon z_{i-1}^{[1]} + (1 - \epsilon) z_{i-1}^{[2]} \right] + \alpha_2 z_{i-2}^{[2]} + a_i^{[2]} - \beta_1 a_{i-1}^{[2]} - \beta_2 a_{i-2}^{[2]},
\end{aligned}
$$

where $\alpha_1 = 1.90693$, $\alpha_2 = -0.98751$, $\beta_1 = 0.78512$, $\beta_2 = -0.40662$ and $a_i^{[j]}$ are independent and identically distributed Gaussian random variables with zero mean and standard deviation 0.4. The conditional mutual information $I(z^{[1]}; z_T^{[2]} | z^{[2]})$ and $I(z^{[2]}; z_T^{[1]} | z^{[1]})$ ($z_T^{[i]}$ denotes the time series $z^{[i]}$ shifted by T samples into the future) can be computed analytically [61]. For a set of variables $X_1, X_2, ..., X_n$ having zero mean, unit variance and correlation

matrix C, their mutual information can be computed as

$$I(X_1, X_2, ..., X_N) = -\frac{1}{2} \sum_{i=1}^{N} \log(\sigma_i),$$

where σ_i are eigenvalues of the correlation matrix C. The conditional mutual information can be computed using mutual information according to (2.5). Long time series ($> 10^6$ samples) were used to compute the analytical estimates ensuring that they have a negligible bias and variance with respect to the non-parametric methods.

In Fig. 2.1 the convergence behavior with respect to the free parameter of the method is shown as a variable dependent on the amount of data provided as input to the method. It should be noted that the raw (normalized) time series were processed as the properties of the estimators are under investigation in this test. While the B-spline estimate is severely negatively biased for the selected bin counts, the bias of the Equiquantal estimator changes from positive to negative as the amount of supplied data increases. It should be noted that the B-spline estimator is very expensive in terms of computational effort so higher B-spline curve orders or bin counts take a very long time to compute. The cross-redundancy estimator, which is metric based, converges to a value dependent on the size of the neighborhood, it is ease to see that larger neighborhoods introduce more negative bias into the estimation.

From the above results, it is clear that none of the supplied methods can be relied upon to provide an estimate of the true value of the conditional mutual information functional, much less so for short time series. Except time series length, estimator type and free parameter setting, the estimates of conditional mutual information are also dependent on the amount of noise in the source time series, the complexity of the dynamical systems, their relative parameters and structure. It is thus difficult to decide on the directionality from the values of the indices alone except under favorable circumstances where strong assumptions about the individual dynamics and character of the time series can be made. Tests on model systems indicate that when the systems are very similar in structure and parameters, the indices may be
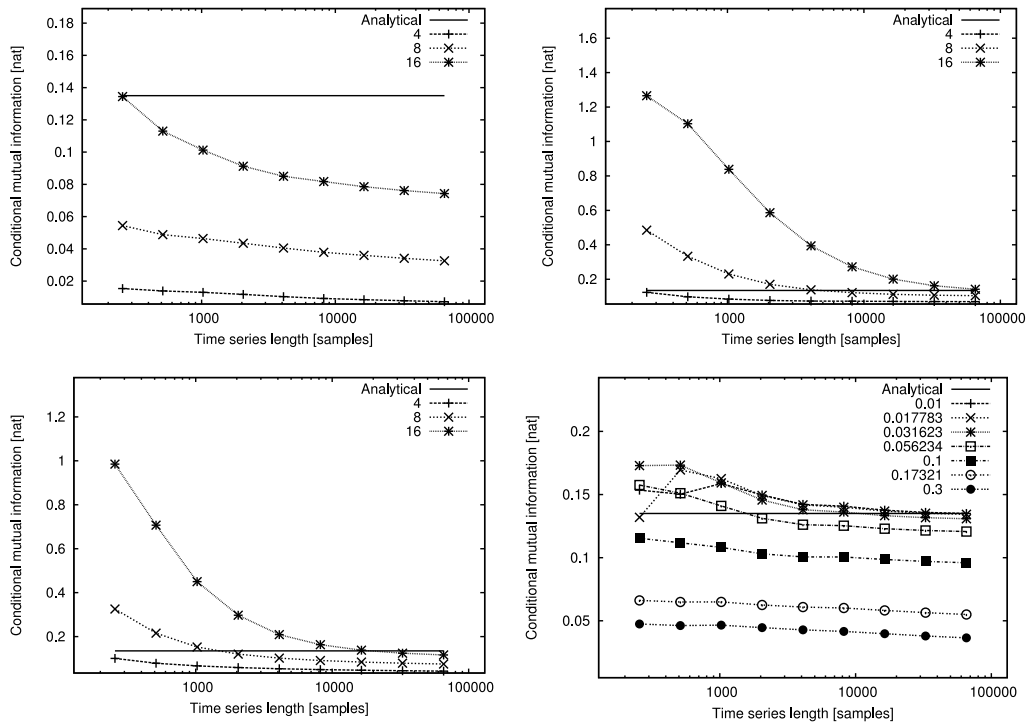
Figure 2.1: Convergence behavior of CMI estimators vs. length of input series with respect to their free parameter on the Barnes model using the B-spline method (top left), using the Equiquantal estimator (top right), the cross-redundancy estimator (bottom left) and the classical histogram estimator (bottom right). The horizontal full line indicates the analytically computed conditional mutual information.

directly used as an indicator of the asymmetry of coupling.

Chapter 3

Quantifying dependent states

Quantification of various synchronization types is a much more intensively studied problem than the detection or quantification of directionality. One of the most important types of synchronization studied in oscillatory systems is *phase synchronization* which is a process of mutual attunement of rhythms of two oscillating systems. Phase synchronization can occur under very weak coupling and has been found in stochastic systems and even in systems exhibiting deterministic chaos [1].

The only method to verify without doubt that a pair of systems exhibits phase synchronization is to perform an *active experiment*. If two systems are apparently oscillating in synchrony, a disturbance should be introduced in the behavior of at least one of the systems. If the systems thereafter resume their synchronous motion (after a transient period), then it can be asserted that phase synchronization is taking place. Frequently, an active experiment cannot be performed, either because there is no feasible way to disturb the systems, it is unethical (e.g. in health care) or the experiment has been performed in the past and only a record in the form of time series is available. At this point, specialized techniques of time-series analysis are required to handle the problem.

The situation is further complicated by the fact that multiple paths to synchronization have been discovered. The same systems with slightly different parameters can exhibit markedly different behavior when coupling is

increased. For example the Rössler chaotic oscillator has been investigated
by Rosenblum *et al.* [1] and Fig. 3.1 summarizes their findings about paths
to synchronization for a pair of symmetrically coupled Rössler systems

$$
\begin{aligned}
\dot{x}_{1,2} &= -\omega_{1,2}y_{1,2} - z_{1,2} + \epsilon_{1,2}(x_{2,1} - x_{1,2}) \\
\dot{y}_{1,2} &= \omega_{1,2}x_{1,2} + 0.15y_{1,2} \\
\dot{z}_{1,2} &= 0.2 + z_{1,2}(x_{1,2} - 10)
\end{aligned}
\qquad , \qquad (3.1)
$$

where $\epsilon_{1,2}$ is the coupling strength.
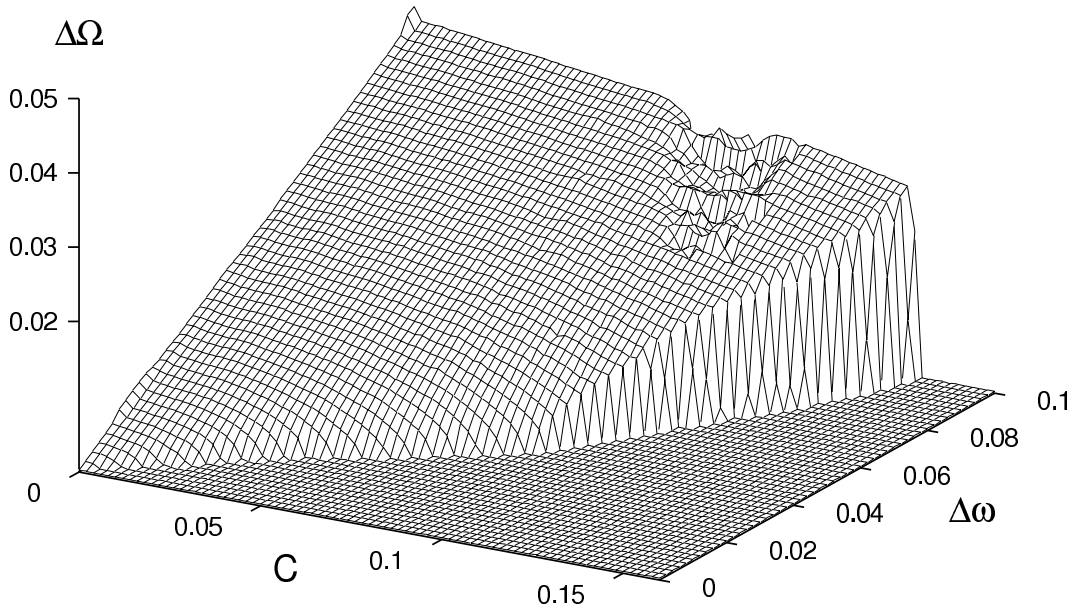
Figure 3.1: The relative phase velocity of two slightly detuned symmetrically
coupled Rössler systems (3.1). The coupling strength is represented by $C = \epsilon_{1,2}$ and $\Delta\omega$ is the frequency detuning $\omega_{1,2} = 1 \pm \Delta\omega$. When the systems
are phase synchronized, the difference in phase velocities is 0. Note that
for different detuning parameters, the transition is either abrupt or gradual.
[Image from Rosenblum *et al.* [1], used with permission.]

In Fig. 3.1 the (symmetric) coupling strength is represented by $C = \epsilon_{1,2}$
and $\Delta\omega$ is the detuning $\omega_{1,2} = 1 \pm \Delta\omega$. The Rössler systems in the config-
uration described above exhibit either a gradual or an abrupt transition to
synchronization with respect to changing coupling strength. This depends on
the original detuning of their natural frequencies $\omega_{1,2}$ — for small detuning,

the transition is gradual, while for higher detuning, the transition occurs at a higher coupling strength but is more abrupt. In general however there is a threshold of synchronization for each pair of systems and set of parameters (if the systems do synchronize). The situation with respect to changing coupling strength if all other parameters are fixed is depicted in Fig. 3.2.
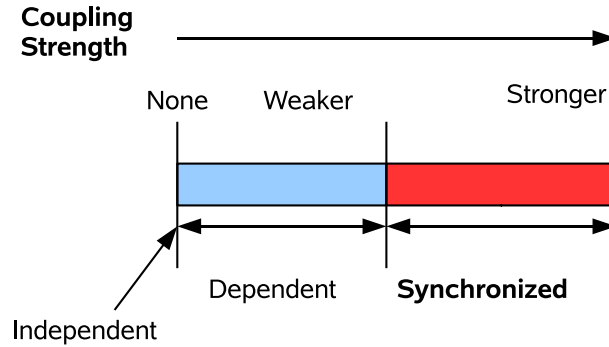
Figure 3.2: A depiction of a typical transition to synchronization. With no coupling (whether uni- or bidirectional), the systems are independent. As the coupling strength is increased, the systems become more dependent. When a threshold is passed, the systems align their rhythms and synchronize.

3.1   Definitions of phase synchronization

There is a certain dichotomy surrounding the concept of phase synchronization. In theory [62, 2], mathematical definitions exist to describe synchronized systems and the effect of synchronization on their states. In time series analysis, however, synchronization is often interpreted as a statistical phenomenon, leading to the quantification of a "degree of synchronization".

The criteria of synchronization that follow make use of the definition of the *generalized phase difference*

$$\psi_{\mathrm{mn}} = m\phi_1 - n\phi_2, \tag{3.2}$$

where $\phi_{1,2}$ are the instantaneous phases describing the motion of the two systems, ψ_{mn} is the generalized phase difference and $m{:}n$ is the locking ratio. Where appropriate, the subscripts m and n are dropped to simplify the

notation. The *wrapped phase difference* is defined as

$$\Psi_{\mathrm{mn}} = \psi_{\mathrm{mn}} \mod 2\pi. \tag{3.3}$$

The condition for phase synchronization is usually given in the form [2]

$$|\psi_{\mathrm{mn}}| < \mathrm{const.} \tag{3.4}$$

This condition is only applicable to infinite time series and is not easily tested in practice as any finite time series will exhibit some maximum difference whether the two systems synchronize or not. There have however been attempts to derive upper bounds on the phase difference for synchronized systems [63]. Another definition given in [2] is denoted *frequency locking* and is slightly weaker than the bounded phase difference condition. The condition can be stated as

$$m\langle\dot{\phi}_1\rangle = n\langle\dot{\phi}_2\rangle, \tag{3.5}$$

where $\langle\cdot\rangle$ denotes the time average. The condition can also be rewritten as

$$\langle\dot{\psi}_{\mathrm{mn}}\rangle = 0. \tag{3.6}$$

When analyzing experimental data, indices quantifying the *degree of synchronization* [13, 22, 64, 61] are often applied to the time series. It should be noted that although these indices quantify the dependence between the two systems, they are generally not connected to either of the above definitions of phase synchronization. The name synchronization index is thus misleading and a better-suited name would be 'dependence index'. If the index grows monotonically with the strength of coupling (degree of dependence) between the systems then there exists for a particular pair of systems and a specific set of conditions a critical value of the index. If the index computed for a given pair of time series exceeds this value, the systems are synchronized. However, this critical value depends on practically all the system parameters. Thus a procedure to compute the critical value for a given setting is

needed to turn a dependence index into a robust detector of synchronized states. Up to date there have been some attempts to automatically find such a threshold using the well-established method of surrogate data [33, 32, 65], which will be elaborated in the next Chapter.

In the following, a selection of phase dependence indices will be briefly described and their behavior will be elucidated on a pair of Rössler oscillators which exhibit deterministic chaos.

3.2   Indices of phase dependence

In the following, various indices of phase dependence are introduced and briefly described. It is again noted that none of these 'dependence indices' has been derived from either of the definitions of phase synchronization (3.5) or (3.6). The indices typically reflect the existence of a relationship between the distributions of the phases. Each of the subsequent methods is effectively a non-directional index of interdependence.

3.2.1   Conditional probability

Tass *et al.* [22] have proposed an index based on *conditional probability* which characterizes the dependency of the distributions of the phases of both analyzed systems. The wrapped phase interval $\langle 0, 2\pi \rangle$ is divided into M subintervals — bins. For each subinterval $1 \leq j \leq M$ the index

$$r_j = \frac{1}{N_j} \sum_{k, \phi_1(k) \in b_j} e^{i\phi_2(k)}, \qquad (3.7)$$

is computed, where b_j denotes the bin corresponding to the j-th subinterval and N_j is the number of points $\phi_1(k)$ belonging to b_j. As the dependency grows stronger $|r_j| \to 1$, for vanishing dependencies $|r_j| \to 0$. The average value of r_j over all the bins b_j results in the index

$$\lambda = \frac{1}{M} \sum_{j=1}^{M} |r_j|. \qquad (3.8)$$

The number of bins used to quantize the input phase series is a free parameter of the conditional probability index.

3.2.2 Mean phase coherence

Mean phase coherence has been proposed in Ref. [64] and was based on a complex order parameter defined by Kuramoto [66] to characterize ensembles of oscillators. The index has been applied to broadband electroencephalographic data in [13]. Later it was linked to circular variance [67] by Allefeld and Kurths [68]. The index is defined as

$$R = \frac{1}{N} \left| \sum_{j=1}^{N} \exp i\psi_{mn}(j) \right| = 1 - CV, \qquad (3.9)$$

where CV denotes the circular variance. The index is related to the spread of the distribution of phase differences on the space $\langle 0, 2\pi \rangle$ with circular topology. If the distribution is narrow, then the circular variance is small and the index $R \to 1$. For a wide nearly-uniform distribution $R \to 0$. Mean phase coherence is computed from the phase differences of unwrapped phases and has no free parameters.

3.2.3 Mutual information

Mutual information [69] is an established measure of non-linear dependency between ensembles of data. There is a number of methods to estimate mutual information from time-series. The classical binning (boxing) approach and its various modifications [45, 46, 61] are still widely applied due to their robustness, simplicity and performance (cf. Sec. 2.2.1). These *binning* approaches map the data points into a discrete sets of values Ξ, Υ, from which mutual information can be computed using

$$I(X;Y) = H(X) + H(Y) - H(X,Y), \qquad (3.10)$$

where $H(X), H(Y)$ are entropies of the time series X and Y respectively and $H(X, Y)$ is their joint entropy

$$
\begin{aligned}
H(X) &= -\sum_{x \in \Xi} p(x) \log p(x) \\
H(Y) &= -\sum_{y \in \Upsilon} p(y) \log p(y) \\
H(X, Y) &= -\sum_{x \in \Xi, y \in \Upsilon} p(x, y) \log p(x, y)
\end{aligned}
$$

(3.11)

The most basic histogram approach divides the space into M intervals of the same length and assigns each point to the bin representing the interval to which it belongs. This approach (equidistant binning) and its theoretical properties have been investigated by Moddemeijer [45]. A modification of the above approach exhibiting better statistical properties is the method of equiquantal binning which splits the dataset into intervals (bins) so that each bin contains the same amount of points [61]. This method is included in the subsequent numerical study. The number of bins M is a free parameter of the method.

Recently a new approach to estimate mutual information based on nearest neighbor distances was proposed by Kraskov et al. [70] based on the previous work of Kozachenko and Leonenko [71]. Here mutual information is estimated directly, without recourse to entropies or the probability density function using

$$
I(X; Y) = \psi(k) - \langle \psi(n_x + 1) + \psi(n_y + 1) \rangle + \psi(N), \tag{3.12}
$$

where ψ denotes the digamma function and $\langle \cdot \rangle$ denotes the sample average. To estimate mutual information, each point is used as a reference point and its k-th nearest neighbor is found in the joint space (X, Y). Its distance from the reference point is used to define a hypersphere around the projection of the reference point into the subspaces X and Y. The numbers n_x and n_y denote the number of points in the hyperspheres in the subspaces X and Y respectively. The authors of [70] have also proposed an alternative

estimator of mutual information based on hyper rectangles. The estimator (3.12) is included in the numerical study in this work. The number of nearest neighbors k used to estimate mutual information is a free parameter of the estimator.

3.2.4   Shannon entropy of the phase differences

Shannon entropy of the phase differences was proposed by Tass *et al.* [22] and requires that the entropy of the generalized phase differences is estimated. The index is computed as

$$\tilde{\rho}_{nm} = \frac{S_{\max} - S}{S_{\max}} \tag{3.13}$$

where

$$S = -\sum_i p_i \log p_i$$

and $S_{\max} = \log M$, where M is the number of bins and p_i denotes the probability of the wrapped phase difference Ψ_{mn} falling into the i-th bin. The index ρ_{mn} is constrained to the range $\langle 0, 1 \rangle$. The value 0 is associated with a uniform distribution of the phase differences and 1 corresponds to all of the phase differences being assigned to the same bin. The more peaked the distribution of phase differences is, the more constrained the wrapped phase differences are and this should correspond to the phases being more dependent. The number of bins M is a free parameter of the method.

3.3   Example results

Detailed numerical experiments have been performed on coupled Rössler systems to test how the above methods react to increasing strength of coupling. The equations for the linearly coupled Rössler pair have already been given (3.1). In this example, the x coordinate was selected as the observable from which phase was derived. A Runge-Kutta 4th order scheme was used to integrate the oscillators with a time step of 0.01 s, the resulting time series

was sub-sampled by a factor of 10 to yield a time series with ≈ 60 points per period.

Phase was extracted by constructing a two dimensional time-delay embedding from the x coordinate. This is similar to using a projection of the attractor into a plane spanned by two selected coordinates and taking the angle of the line from the origin to the current position of the system state in this plane as the instantaneous phase [72].

A selection of computational results is in Fig. 3.3. It is clear that all the indices exhibit a monotonous dependence on the strength of coupling (up to some small fluctuations). This is a desirable property. Ideally, the (normalized) index should stay close to zero for couplings smaller than the synchronization threshold and very quickly rise to its maximum value just after the synchronization threshold. Some of the indices conform to this ideal characteristic more, some less as can be seen in Fig. 3.3.
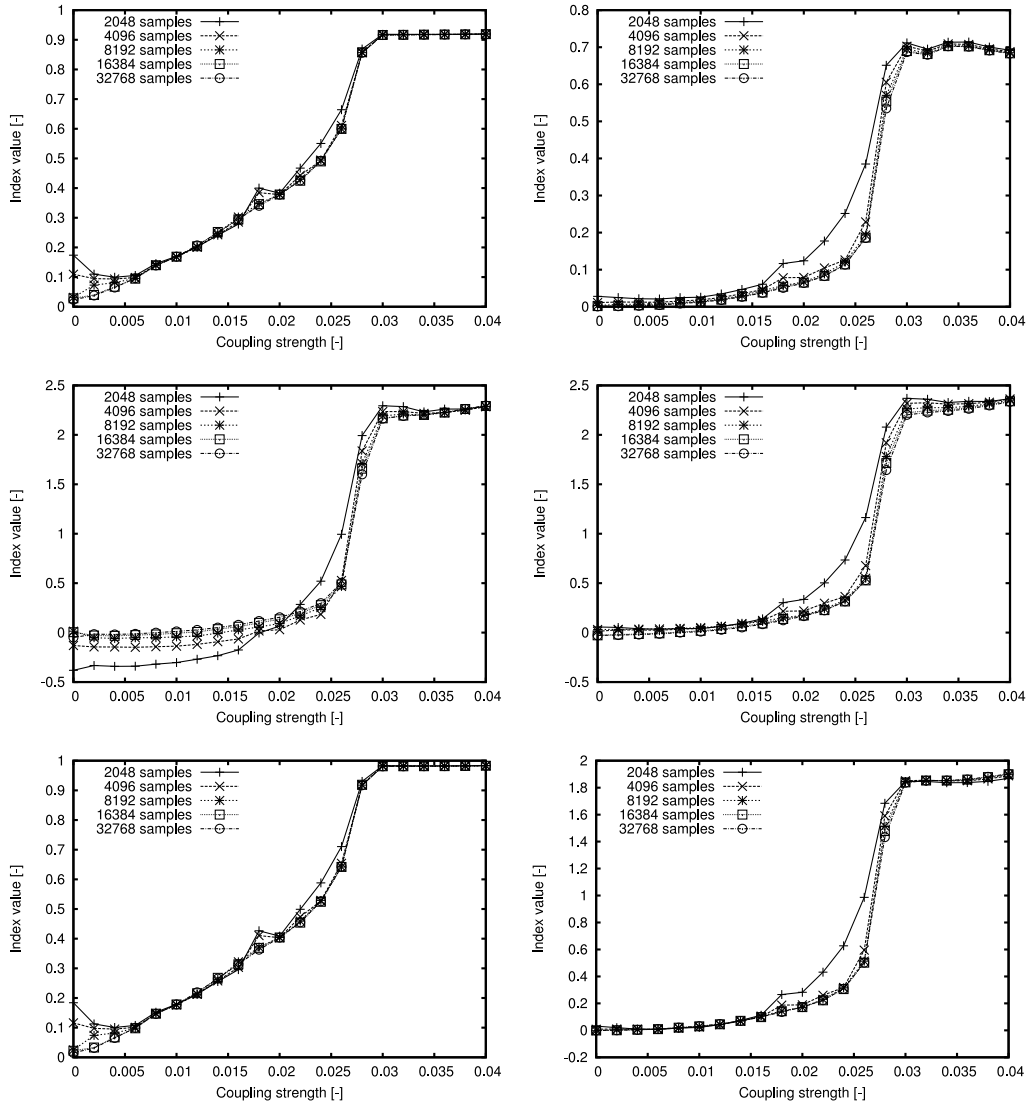
Figure 3.3: Index value vs. coupling strength for different time series lengths: conditional probability with 16 bins (top left), entropy of phase differences with 16 bins (top right), Kraskov *et al.*'s estimator of mutual information using 1st neighbor (center left), 16th neighbor (center right), mean phase coherence (bottom left) and binned mutual information (bottom right). Synchronization threshold is approximately at strength of coupling $\epsilon_{1,2} = 0.027$.

Chapter 4

Testing the significance

In Chapter 2 different methods to quantify directional interactions have been discussed and in Chapter 3 methods estimating the amount of statistical dependence between two time series have been introduced. However these values may be biased by estimator properties, by the amount of noise in the time series, by the complexity and characteristics of individual dynamics of each system. The absolute values of the results of the above algorithms thus have no clear interpretation except in special circumstances.

Additional algorithms must be supplied to test whether the obtained value of an index is a significant indication of directional coupling or dependence. A frequently used approach to the verification of significance of an index value is the method of *surrogate data* [33]. Surrogate data in this context are time series which preserve all the properties of the original time series except the one which is being tested. In both cases (directionality and synchronization), the tested property is coupling. Surrogate time series would thus ideally be series measured from the same systems when it is known that they are not coupled.

In this Chapter we will concentrate on the standard passive experiment where only the time series of two systems are available. In this case, surrogates conforming to the above criteria are very difficult to construct from a single pair of time series with limited length. Let us suppose that the underlying model of both of the observed dynamical systems is known and

available. Given a fixed coupling strength, if two pairs of time series from random initial conditions are generated and the first time series is taken from the first pair and the second time series from the second pair, the resulting pair of time series has the same dynamics as a pair at the given coupling strength but each system is fully independent of the other system. The dynamics are thus replicated exactly and there is clearly no coupling between the systems. These surrogates have been called equation-based surrogates [73].

Testing directionality or dependence algorithms is performed on known models and the above "ideal" surrogates can be readily constructed. These surrogate series shall be considered a benchmark or ideal surrogates against which other surrogate generation algorithms will be compared. If the models
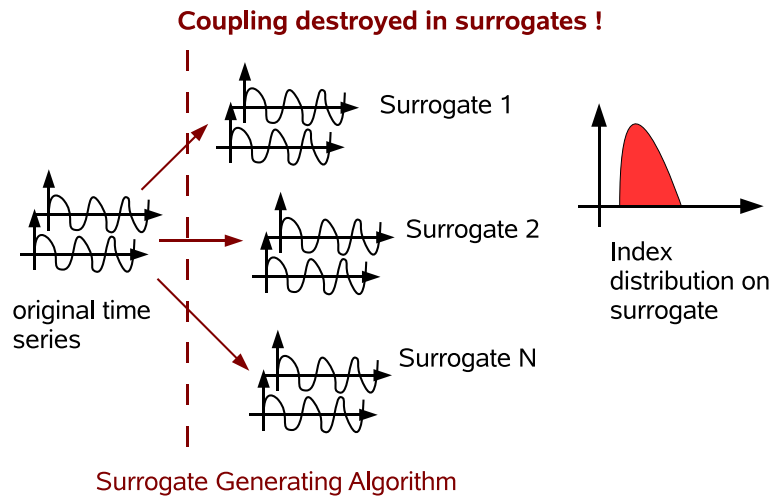
Figure 4.1: Schema of the process of generating surrogates.

of the underlying systems are not available, as is the case with experimental data, there are a some algorithms that can be used to construct surrogate time series. These algorithms are the subject of ongoing research and none of them are close to the best possible surrogates described above or are very difficult to apply in practice. The input of these algorithms is the original time series and the output is the desired number of surrogates as shown in Fig. 4.1.

4.1 Hypothesis testing

Assuming that applicable surrogates are available, a standard one sided hypothesis test can be constructed to check whether an index value is significant. The hypothesis test is understood as a Neyman-Pearson decision problem [74]: directionality should be detected as often as possible (high true positive rate) under the condition that the false positive rate (detected coupling when there is none) is less than a given fraction, usually 5%.

The null hypothesis is that the two systems are not coupled in the direction in which directionality is being investigated. Based on the evidence in the time series an attempt is made to reject this hypothesis. Assuming that a bivariate time series is available, the test is performed as follows: the indices $i_{X \to Y}$ and $i_{Y \to X}$ are evaluated on a predetermined number of surrogate datasets generated from the bivariate time series, whence an estimate of the cumulative distribution function (CDF) of each index can be obtained. This distribution represents the variability of the directionality indices $i_{X \to Y}$ and $i_{Y \to X}$ for "independent" systems (i.e. under the null hypothesis). For an apriori selected level of significance, typically 5%, it is possible to obtain critical values for the indices from both of the CDFs. If the value of the index obtained from the original (possibly coupled) bivariate time series is higher than the associated critical value, it is significant at the chosen significance level and directional influence in the direction corresponding to the index has been detected. If the value of the index is not significant then the evidence in the time series does not support rejecting the null hypothesis of no coupling in the given direction.

If the generating systems do not vary with time, it is possible to precompute thresholds from the surrogates which ensure detection of directional influence at given levels of significance. Some frequently used surrogate generation methods are described in the following paragraphs.

4.2 Techniques for creating surrogate data

4.2.1 Fourier transform surrogates

Fourier transform surrogates are constructed by computing the Fourier transform of each time series, randomizing the phase of each frequency component (except the component corresponding to frequency 0, which must have 0 phase) and then taking the inverse transform. In practice this is accomplished by computing the Fast Fourier Transform (FFT) [75] of the time series and there are many software packages available that provide required procedures. The autocorrelation function and spectrum are preserved but the distribution of amplitudes is usually slightly flattened [33]. Further improvements on the basic method try to iteratively converge upon surrogates that more accurately match the original frequency spectrum and the original amplitude distribution at the same time [32].

4.2.2 Permutation surrogates

Permutation surrogates have been previously applied to phase time series obtained using the marked events method [76, 77]. The sequence of durations (intervals) of each cycle of the time series is first extracted. The intervals are then randomly reordered and a new phase time series is constructed based on the reordered sequence. The process is repeated until the desired number of surrogate time series is obtained.

For instantaneous phase, essentially the same procedure applies but care must be taken to preserve the intra-period information in the signal. The signal is first divided into periods and all the periods except the first and last are shuffled randomly. The first and last period are not displaced because this would create discontinuities in the surrogate signal as usually only a part of the first and last period is available. The distribution of phases is preserved when this method is applied. The procedure is illustrated in Fig. 4.2

This procedure has been applied in the present work as the comparison includes methods which are dependent on the distances between data points whence it is important to preserve the distribution of phases as accurately
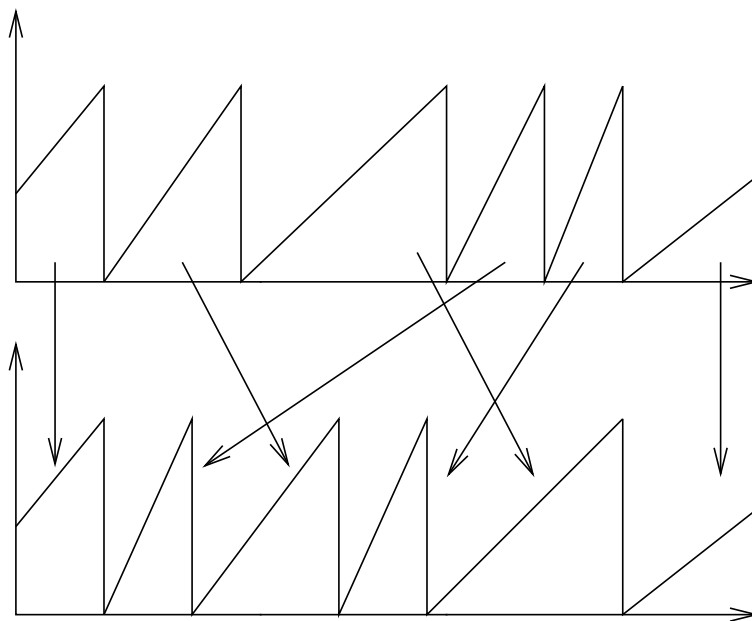
Figure 4.2: The procedure of shuffling individual cycles in a wrapped phase signal.

as possible. We note that permutation surrogates differ from the 'white noise' or 'scrambled' surrogates where the time-series samples are simply reshuffled randomly yielding a time-series which preserves the distribution but completely destroys any structure in the time series.

4.2.3   Twin surrogates

Recently the technique of analyzing non-linear dynamical systems using recurrence plots [78, 79] has gained some popularity. Recurrence plots (RPs) indicate instances of time when the trajectory of the dynamical system passes close to a point it has visited previously. A recurrence plot of a process can be used to construct *twin surrogates* [73] by exploiting special points which are equivalent with respect to the recurrence plot. A twin surrogate is a time series which is constructed by reordering segments of the original time series so that the reordering does not alter the recurrence plot. Since several important quantities are derivable from recurrence plots, the equivalence of recurrence plots ensures that these quantities remain unchanged between

the original data and the surrogate (up to a precision dependent on the resolution of the recurrence plot and the amount of data). The application of recurrence plots to univariate time-series however requires that a state-space reconstruction technique such as time-delay embedding [8] is applied prior to the construction of an RP.

4.3 The complete method

A summary of the current method of processing time series attempting to detect the investigated interactions is shown in Fig. 4.3.
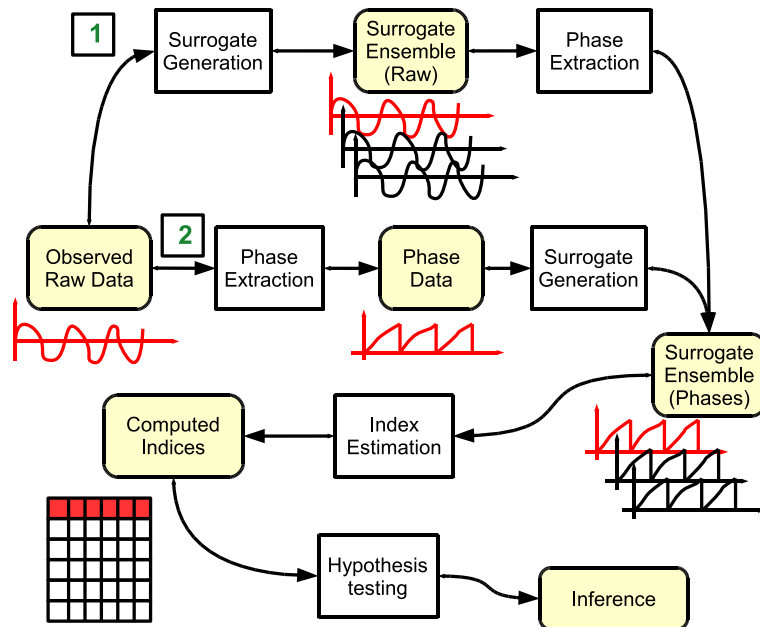
Figure 4.3: The processing pipeline from raw data to the inference on directionality/dependence. If raw data is needed for surrogate generation (as with e.g. FFT surrogates), branch $\boxed{1}$ is selected. For surrogates requiring phase time series, branch $\boxed{2}$ is used, this is the case with permutation surrogates.

The raw data (pair of time series of observables) must be processed to obtain phase signals, this process is briefly touched upon in the introduction 1. The phase is then analyzed using the selected index and estimation method as described in Chapters 2 and 3. A fixed number of surrogates is generated to

estimate the distribution of the index under the null hypothesis as described in this Chapter. Depending on the result of the hypothesis test, a final inference is made. If the index resulting from the experimental time series was found significantly different from the distribution of indices under the null hypothesis, the result is significant and coupling in the given direction has been detected. The test is repeated for the opposite direction. As a result of this construction, two independent decisions indicating the existence of coupling in either direction are available.

Chapter 5

Original contributions

In this Chapter, the original contributions to both detection problems are presented.

5.1 Directionality analysis

Based on previous work of Kozachenko and Leonenko [71] on entropy estimates from nearest neighbor distances, Kraskov *et al.* [70] have derived an estimator of mutual information from k-th nearest neighbor distances. Recently, Goria *et al.* [80] has shown that entropy estimators based on k-th nearest neighbor distances are consistent. The derivation of a k-th nearest neighbor (k-NN) estimator of mutual information in [70] based on the work [71] is introduced because the same rationale has been applied to deriving a conditional mutual information estimator.

The developments follow [70] and are based on [71, 81, 82]. Assuming that there are two processes $\mathcal{X}$ and $\mathcal{Y}$ which have been measured and a record of their activity is in time series with the sample space X and Y respectively. A metric needs to be defined in each sample space. The space (X, Y) is the joint sample space for which a metric must be available. In the development of the algorithm, the max norm $|| \cdot ||_{\text{inf}}$ was used in all cases but the form of the algorithm does not depend on the metric.

The Shannon (differential entropy) is defined as

$$H(X) = - \int \mu(x) \log \mu(x) dx, \tag{5.1}$$

where $\mu(x)$ is the probability density function on the sample space X. The formula (5.1) can be understood as an average of the quantity $\log(\mu(x))$. If it would be possible to construct an estimator $\widehat{\log(\mu(x))}$, we could then estimate the Shannon entropy as

$$H(X) = \frac{1}{N} \sum_{i=1}^{N} \widehat{\log(\mu(x_i))}, \tag{5.2}$$

where N is the number of samples available and x_i denotes the i-th sample (vector). The derivation of the $\widehat{\log(\mu(x))}$ estimator is based on the probability $P_k(\epsilon)$ for the distance between the reference point x_i and its k-th neighbor. Let the probability $p_i(\epsilon)$ be the mass of the ϵ ball centered at x_i

$$p_i(\epsilon) = \int_{||\xi - x_i|| < \epsilon/2} \mu(\xi) d\xi. \tag{5.3}$$

The probability $P_k(\epsilon) d\epsilon$ corresponds to the probability that there is exactly one point in the range $[\epsilon/2, \epsilon/2 + d\epsilon/2]$ and that there are $k - 1$ points closer to x_i and $N - k - 1$ points farther from x_i. With the help of $p_i(\epsilon)$ this probability can be expressed as

$$P_k(\epsilon) = \frac{(N-1)!}{1!(k-1)!(N-k-1)!} \frac{dp_i}{d\epsilon} \times p_i^{k-1} \times (1 - p_i)^{N-k-1}, \tag{5.4}$$

which is the multinomial formula applied to the above problem. This can be simplified to

$$P_k(\epsilon) = k \binom{N-1}{k} \frac{dp_i}{d\epsilon} \times p_i^{k-1} \times (1 - p_i)^{N-k-1}. \tag{5.5}$$

The expectation value of $\log p_i(\epsilon)$ is then computed as

$$
\begin{aligned}
E[\log p_i] &= \int_0^\infty P_k(\epsilon) \log p_i(\epsilon) d\epsilon \\
&= k \binom{N-1}{k} \int_0^1 p^{k-1}(1-p)^{N-k-1} \log p \; dp \\
&= \psi(k) - \psi(N),
\end{aligned}
\tag{5.6}
$$

where the expectation is computed with respect to a fixed reference point x_i. A simplifying assumption is now made that $\mu(x)$ is constant over the entire ϵ ball. Then

$$
p_i(\epsilon) \approx c_d \epsilon^d \mu(x_i),
\tag{5.7}
$$

where d is the dimension of x and c_d is the volume of the d-dimensional unit ball. Now the estimator of $\log \mu(x_i)$ can be written as

$$
\log \mu(x_i) \approx \psi(k) - \psi(N) - dE[\log \epsilon] - \log(c_d),
\tag{5.8}
$$

whence Shannon entropy can be estimated

$$
\hat{H}(X) = -\psi(k) + \psi(N) + \log c_d + \frac{d}{N} \sum_{i=1}^N \log \epsilon(i)
\tag{5.9}
$$

It is clear that this estimate is biased by the assumption that $\mu(x_i)$ is constant in the entire ϵ ball.

To derive the mutual information estimator

$$
I^{(1)}(X, Y) = H(X) + H(Y) - H(X, Y).
\tag{5.10}
$$

of Kraskov $et\ al.$ [70] the logic of the above estimate is further manipulated to reduce its bias. It would be indeed possible to apply the entropy estimate (5.9) to each term and compose the final result. However the biases in the individual terms would not cancel because in general the distances to k-th neighbors in the joint space (X, Y) would be higher than that in the subspaces X and Y. The non-uniformity of the probability density function in the subspaces X, Y and in the joint space (X, Y) would therefore be

different and cannot be expected to cancel.

To circumvent this problem, Kraskov *et al.* have noticed that (5.8) holds for any value of k and that it is not necessary to select the same value of k for all reference points x_i. The same value of k was used in deriving (5.9) but it is also possible to estimate the entropy using

$$\hat{H}(X) = -\frac{1}{N} \sum_{i=1}^{N} \psi(n_x(i) + 1) + \psi(N) + \log c_d + \frac{d}{N} \sum_{i=1}^{N} \log \epsilon(i), \quad (5.11)$$

where $n_x(i)$ is the number of points inside the hypersphere which intersects the k-th neighbor and ϵ is the diameter of the ball which contains all k points. This can be directly exploited in computing mutual information. The joint entropy is estimated using (5.9) as

$$\hat{H}(X, Y) = -\psi(k) + \psi(N) + \log(c_{d_X} c_{d_Y}) + \frac{d_X + d_Y}{N} \sum_{i=1}^{N} \log \epsilon(i), \quad (5.12)$$

with c_{d_X}, c_{d_Y} volumes of unit balls in the X and Y space, d_X, d_Y the dimensionalities of said spaces and $\epsilon(i)/2$ the distance to the k-th neighbor in the joint space (X, Y). The idea for reducing the bias in estimating mutual information is to use the *same length scale* obtained in the joint space to estimate the densities in the subspaces $\mu(x_i)$ and $\mu(y_i)$.

The entire algorithm then requires that the distance to the k-th nearest neighbor from the reference point (x_i, y_i) is found in the joint space (X, Y). This distance $\epsilon(i)/2$ is the used to find the number of nearest neighbor points in the subspaces X (to obtain $n_x(i)$ points) and Y (to obtain $n_y(i)$ points) which are closer than $\epsilon(i)/2$. Both neighbor counts should be higher than or equal to k. When these neighbor counts are used in (5.11) by inserting the appropriate neighbor count found, one can directly insert all terms into (5.10). Most of the terms will cancel and the final form of the estimator can be written as

$$I^{(1)}(X, Y) = \psi(k) - \langle \psi(n_x(i) + 1) + \psi(n_y(i) + 1) \rangle + \psi(N), \quad (5.13)$$

where $\langle \cdots \rangle$ is the mean over all reference points (x_i, y_i).

Although it would be possible to compute the functional $I(X, Y|Z)$ using the decomposition into multiple mutual information computations as detailed in the introduction (formula repeated here for clarity)

$$I(X, Y|Z) = I(X, Y, Z) - I(X, Z) - I(Y, Z), \qquad (5.14)$$

also in this case biases due to the use of different length scales do not cancel. Our contribution goes further and extends the above reasoning to construct a direct computation of the functional $I(X, Y|Z)$ which requires consideration of distances in the space (X, Y, Z). The computation of conditional mutual information between X and Y, which is conditioned on Z can be split into multiple entropy estimations (2.6).

Following a similar pattern, we shall determine $\epsilon(i)/2$, the distance to the k-th nearest neighbor in the joint (X, Y, Z) space. The same distance scale is then used to find the number of neighbors in the (now multidimensional) subspaces X, (X, Z) and (Y, Z). These nearest neighbor counts will be denoted $n_z(i)$, $n_{xz}(i)$ and $n_{yz}(i)$ respectively. The multidimensional subspaces can be treated in the same way as single dimensional subspaces as only the distances are relevant to the computation. Assuming that the formula (5.11) is used to estimate the individual entropies, the decomposition into multidimensional entropies can be written as

$$
\begin{aligned}
I(X, Y|Z) &= H(X, Z) + H(Y, Z) - H(Z) - H(X, Y, Z) \\
&= \langle \psi(n_z(i) + 1) \rangle + \psi(N) + \log(c_{d_Z}) + \frac{d_Z}{N} \sum_{i=1}^{N} \log \epsilon(i) \\
&+ \psi(k) + \psi(N) + \log(c_{d_X} c_{d_Y} c_{d_Z}) + \frac{d_X + d_Y + d_Z}{N} \sum_{i=1}^{N} \log \epsilon(i) -
\end{aligned}
$$

$$
\begin{aligned}
& -\quad \langle \psi(n_{xz}(i)+1)\rangle - \psi(N) - \log(c_{d_X}c_{d_Z}) - \frac{d_X + d_Z}{N}\sum_{i=1}^{N}\log\epsilon(i) \\
& -\quad \langle \psi(n_{yz}(i)+1)\rangle - \psi(N) - \log(c_{d_Y}c_{d_Z}) - \frac{d_Y + d_Z}{N}\sum_{i=1}^{N}\log\epsilon(i) \\
& =\quad \psi(k) - \langle \psi(n_{xz}(i)+1) + \psi(n_{yz}(i)+1) - \psi(n_z(i)+1)\rangle .
\end{aligned}
\tag{5.15}
$$

Please note that there is no $\psi(N)$ term as it has been canceled out. The estimation of this functional requires a more sophisticated processing system as fast methods for satisfying fixed mass hypersphere queries (finding the k-th nearest neighbor) and fixed range queries (finding all points inside a given hypersphere) must be used. The metric $d_\infty(x,y) = ||x-y||_\infty = \max_i |x_i - y_i|$ is used in this work as it is the simplest to work with and the results seem to converge quicker [70]. Also k-D trees [83] and box indexing algorithms [84] for fast multi-dimensional nearest neighbor search are suited to work with the above metric. Methods for this purpose have been tested on high-dimensional spaces with samples drawn from different distributions and the results have been published in [85].
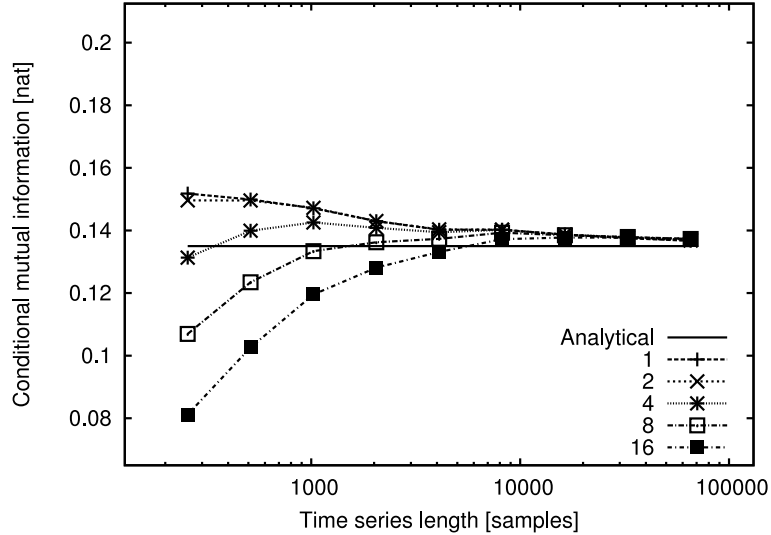
Figure 5.1: Convergence behavior of CMI estimates vs. length of input series with respect to the free parameter on the Barnes model using k-NN method.

The estimator has been tested on the same Barnes model as the methods described in Chapter 2. The estimator of conditional mutual information is based on the theory of k-NN estimation of entropy, which has been shown to be consistent by Goria *et al.* [80]. It is thus expected that this functional will also be a consistent estimator of conditional mutual information. The numerical study supports this assumption as seen in Fig. 5.1 and clearly shows that the method seems to converge for many different values of the free parameter k. This is a unique behavior not seen in any of the previous methods (cf. Fig. 2.1).

5.2   Synchronization analysis

In this section we present an algorithm for detecting phase synchronized states. We show that the frequency locking condition (3.6) for phase synchronization is equivalent to the condition that linear regression of the generalized phase difference has a gradient of zero. This implies that the detection of synchronization from experimental time series reduces to showing that the value of the gradient calculated from linear regression is not significantly different from zero. Determining the significance of the resulting gradient directly would require a knowledge of the statistical properties of the time series and underlying systems which we generally do not possess, therefore we present an alternative technique for determining the significance of the estimated gradient.

In least squares linear regression we write

$$\psi(i) = at(i) + b + \epsilon(i) \tag{5.16}$$

where a and b are chosen to minimize $\chi^2 = \sum_{i=1}^{N} \epsilon(i)^2$ [86, 87]. As a corollary to this we have that mean $\epsilon(i)$ is zero. Subtracting the equations for $\psi(i)$ from the equation for $\psi(i+1)$ and rearranging gives

$$\frac{\psi(i+1) - \psi(i)}{t(i+1) - t(i)} = a + \frac{\epsilon(i+1) - \epsilon(i)}{t(i+1) - t(i)} \tag{5.17}$$

Averaging over all samples and taking the limit $t(i+1) - t(i) = \Delta t \to 0$ gives

$$\langle \dot{\psi} \rangle = a \qquad (5.18)$$

We note that the the above shows that no matter what the actual evolution of the phase difference is, a linear trend will be present if the systems are unsynchronized. The frequency locking condition (3.6) can be restated as $a = 0$. In real time series, noise and fluctuations will invariably cause the value of a to be slightly different from zero. The question is whether the gradient a is significantly non-zero.

The key difficulty with this approach is that the statistical properties of the time series are not known. Phase synchronization detection methods are often applied to complex systems whose physics are poorly understood. Often the only statistical information available is that contained within the time series themselves. Standard methods for calculating the error in linear regression fitting parameters rely on the assumption that the $\epsilon(i)$'s are independent and normally distributed: this assumption is unlikely to be correct. This leads us to the idea of a bootstrap method.

A horizontal line is fitted to the time series using the same approach as previously. The equation for a horizontal line is simply

$$\psi(i) = c + \eta(i), \qquad (5.19)$$

where $\eta(i)$ are the fit errors. The least squares fit is just the arithmetic average $c = \langle \psi(i) \rangle$. Using a least squares fit ensures that $\langle \eta(i) \rangle = 0$. At this point we would like to stress that it is not critical that least squares regression is used. We only require the estimator to guarantee that $\langle \epsilon(i) \rangle = 0$, otherwise the gradient estimate will be biased.

If the two time series are synchronized then there is no real gradient and the value of a extracted from the linear fit is just a random fluctuation. This means that the datasets $\{\psi(i) - c\}$ and $\{\psi(i) - (at(i) + b)\}$ are drawn from the same distribution and, because of the non-zero value of a, one of the datasets is slightly perturbed. On the other hand, if there is a significant gradient in the $\{\psi(i)\}$ then the datasets $\{\psi(i) - c\}$ and $\{\psi(i) - (at(i) + b)\}$

will belong to different distributions.

There is a standard test to verify if two datasets have been drawn from the same distribution—the Kolmogorov-Smirnov test [86, 88]. The test computes the probability that the maximum difference in the cumulative distribution functions estimated from two series will be observed, assuming that they are drawn from the same probability distribution [86]. The test makes no assumptions about the nature of the underlying distribution and is invariant under a reparameterization of the data. In this work we characterize a time series as unsynchronized if the Kolmogorov-Smirnov test gives a probability of less than 5% that the series $\{\psi(i) - c\}$ and $\{\psi(i) - (at(i) + b)\}$ are taken from the same probability distribution.

One disadvantage of the least squares linear regression approach we used is that the calculated parameters can be biased by outliers due to non-gaussian deviations from the linear trend [89, 90]. We expect such outliers to occur in our time series due to the non-linear or chaotic dynamics of the systems and also due to errors in the phase extraction. Long-term correlations (comparable to the length of the time series) also cause spurious rejections of the null hypothesis as sometimes they are detected as a trend. In applications to experimental data, it is likely that measurement error will be a further source of fluctuations. While one option to solve this problem is to try to use a robust estimator, we preferred to use a different approach in which we have inserted an extra step before carrying out the least-squares regression: time indices are sorted by the magnitude of the associated phase difference values. This step leads to a significant reduction in the frequency of false negatives.

If the phase difference series contains a linear trend, the sort will entail "local" mixing only and the autocorrelation function of the phase difference time series is not appreciably changed as shown in Fig. 5.2. If, on the other hand, there is no long-term trend, the series is "globally" mixed thereby significantly changing the autocorrelation function. The most prominent change is that the autocorrelation function drops to zero much quicker than before the mixing. This is exactly what is required to reduce the influence of the correlations on the quality of the LS fit. The effect is clearly seen in
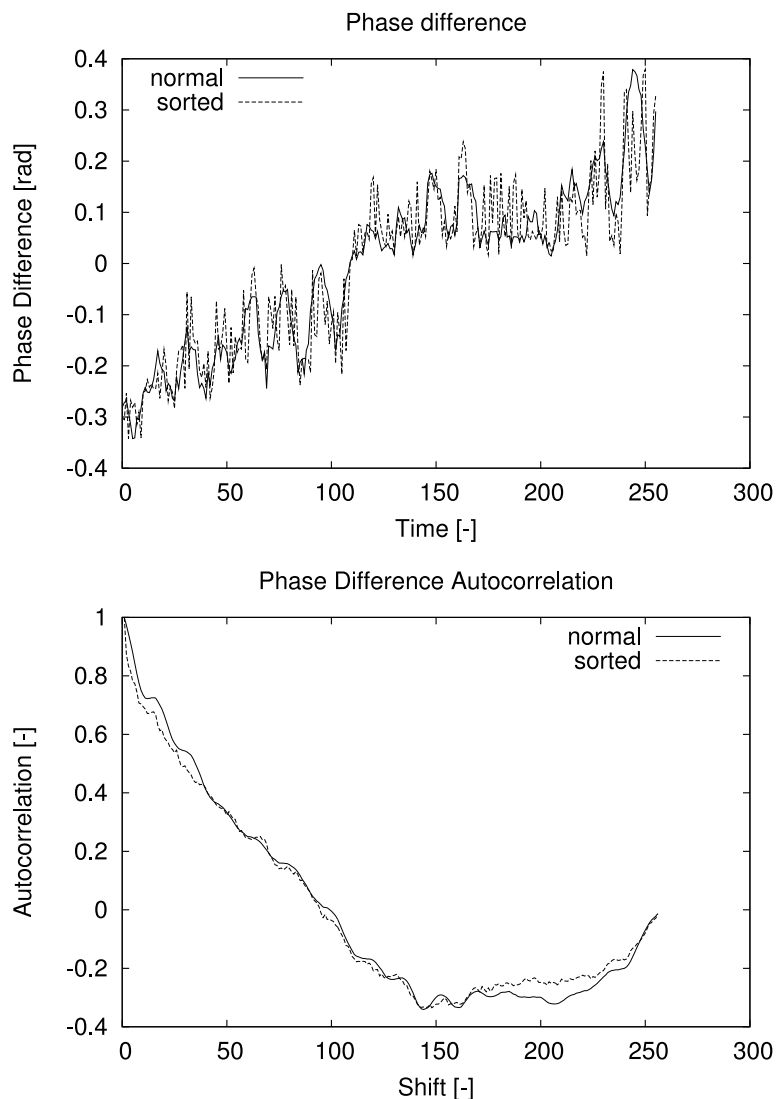
Figure 5.2: Unsynchronized 1:1 Van der Pol oscillators — effect of sorting the time indices by the phase differences.

Fig. 5.3. This procedure causes slightly higher false positives when very noisy series are presented — with intense noise the trend in the phase difference time series becomes obscure and difficult to detect. However, the amount of data required for accurate detection is dramatically reduced and the method becomes highly effective.

To show the effectiveness of the proposed method the same synchronization detection experiment as in section 6.4 was performed using the Bootstrap
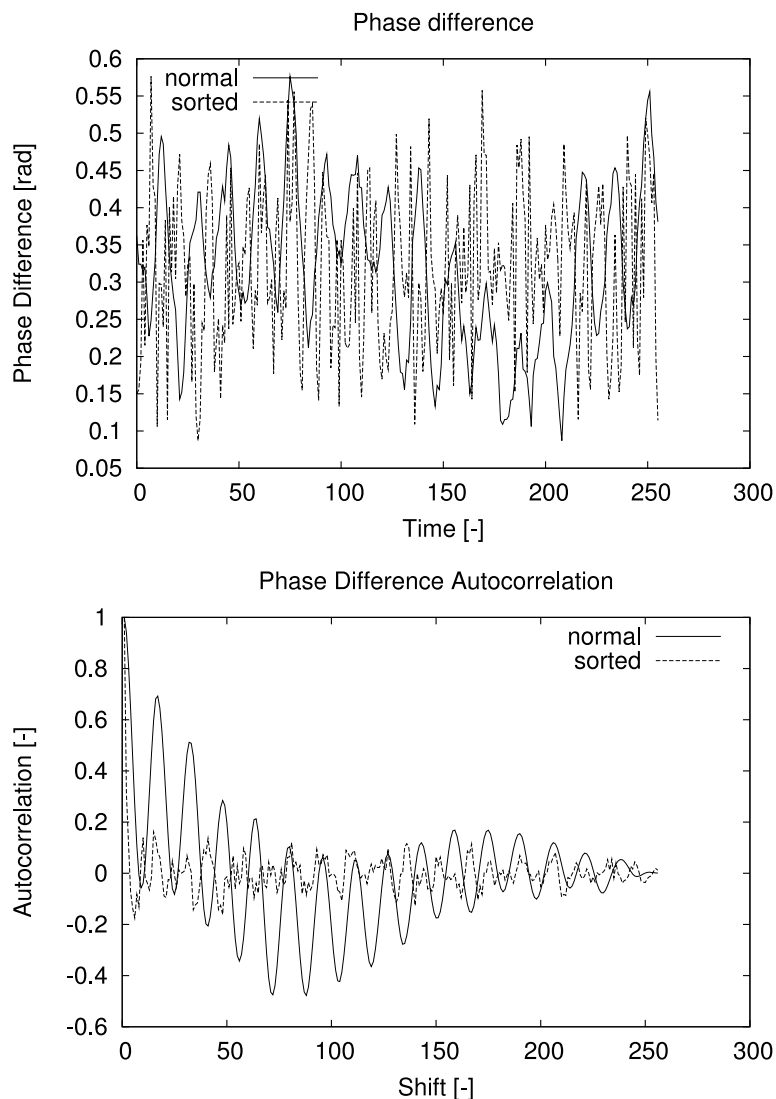
Figure 5.3: Synchronized 1:1 Van der Pol oscillators — effect of sorting the time indices by the phase differences.

phase synchronization detector. The results of the test are shown in Fig. 5.4. No externally generated surrogates are required for the method. The results of the BPSD (Bootstrap phase synchronization detector) method can be compared to those of the previously presented methods by relating Fig. 5.4 to Figs. 6.5, 6.6 and 6.7. Even for short time series, the results of the BPSD method compare favorably to the results of any of the indices coupled with external surrogates. This is due to the fact that a specific definition of syn-

chronization is tested and the null hypothesis is restricted. Indeed, the crucial point is that the BPSD test assumes that the systems are synchronized and uses the evidence in the time series to try to reject it. This turns out to be much easier than the opposite way around, hence the efficacy of the test.
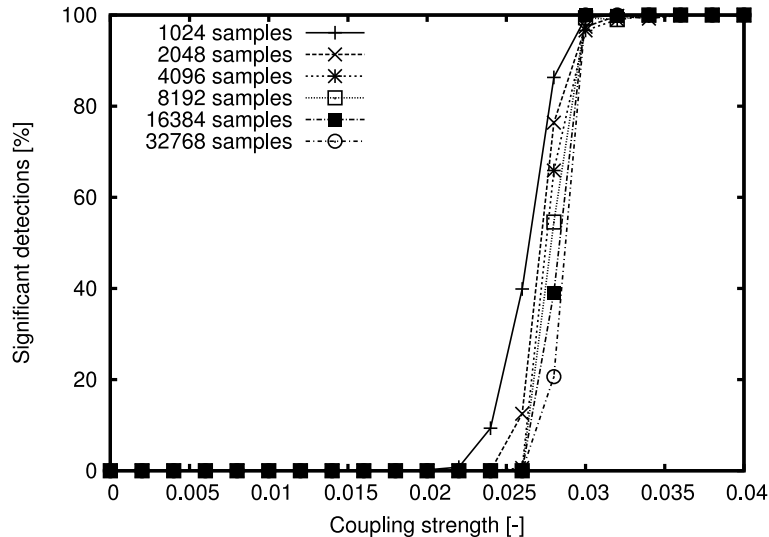
Figure 5.4: Detection rates vs. coupling strength for the symmetrically coupled Rössler pair (3.1) for different amounts of data using the BPSD (bootstrap phase synchronization detector). The synchronization threshold is at $\epsilon_{1,2} \approx 0.027$. Clearly, supplying a longer time series results in an improvement of the detection rates which is not the case in the construction of the synchronization test using a dependence index coupled with a surrogate test. The BPSD detector has very good results even for short time series.

To further explore the properties of the BPSD method previous results of Rosenblum *et al.* [1] have been replicated. In Fig. 3.1, the behavior of the symmetrically coupled Rössler system pair has been shown. The figure is repeated here for reference and comparison in Fig. 5.5 together with the results of detection of synchronization from a time series of length 1024 points. The results of synchronization detection using the BPSD test are in excellent agreement with the results previously published in [1]. In each parameter combination, 512 independent tests were run to estimate the detection rate reliably. In regions with zero relative phase velocity, the detection rate should ideally be 100% and in regions with non-zero relative phase velocity, the de-

tection rate should be 0% as the systems are not synchronized. It is clear that the actual detection rates are very close to these requirements.

(a)

Rossler 1:1 Detection rates

(b)
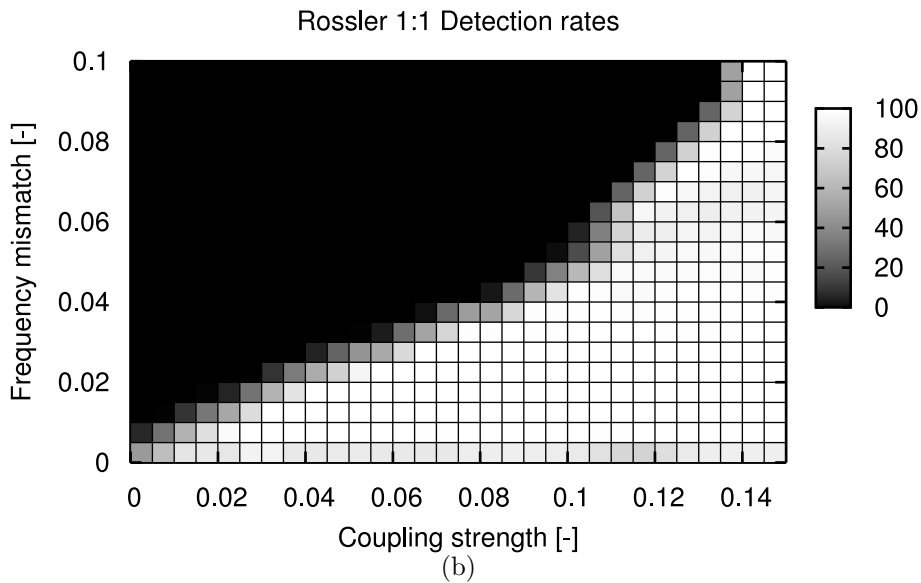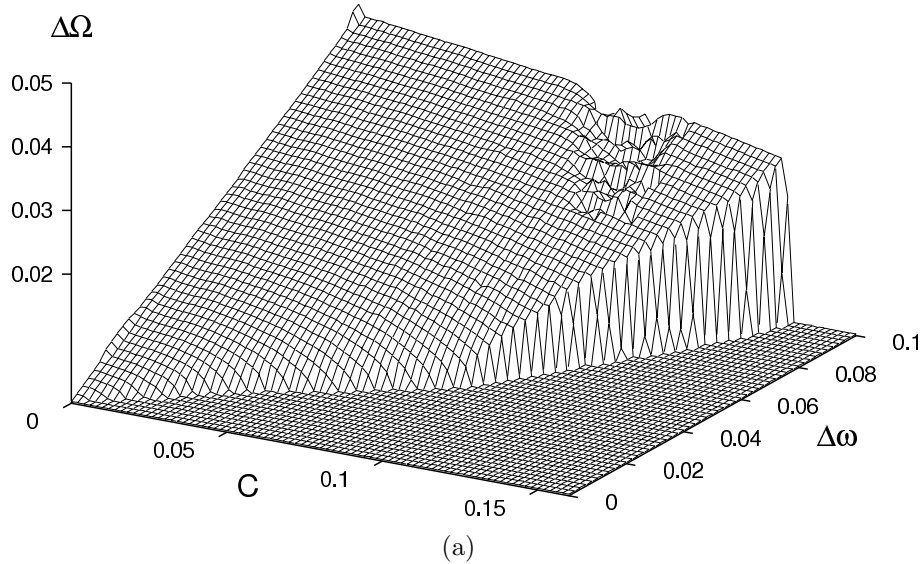
Figure 5.5: Comparison of BPSD test results with previously published results, length of time series was 1024 points ($\approx$ 18 periods). "Coupling strength" corresponds to C and "frequency mismatch" to $\Delta\omega$. On the left, relative phase velocities for each parameter combination have been computed from long time series. When the systems are synchronized, the relative phase velocity is 0, image from [1], used with permission. On the right, results of the BSPD test for the same system parameters. The tests are in clear agreement with the previously published results.

Chapter 6

Numerical studies

In this section we describe detailed numerical studies using a pair of unidirectionally and bidirectionally coupled Rössler systems [29]. The Rössler system is a paradigmatic low-dimensional dynamical system exhibiting deterministic chaos. It is particularly well suited for model experiments because of it's low chaoticity and narrow-band quasi-periodic behavior for some parameter combinations. A coupled pair of Rössler oscillators can be described by the differential equations (3.1).

The basic and well-investigated experimental choice of parameters [1, 41] will be used to investigate several aspects of significance detection. Problems arising in practice will be elucidated using several plots. In the first part, the problem of detecting directionality will be investigated and in the second part, synchronization detection will be treated in detail with respect to surrogate generation methods.

6.1 Directionality: Coupling strength

An index of directionality should increase when the strength of coupling increases. The problem of assigning an absolute strength of coupling between systems which are different in structure or parameters is ill-defined. In the special case of two very similar systems (approximately equal main frequencies, noise levels, dynamics), it is possible to compare the indices of

directionality in both directions. However the behavior of a directionality index can be tested using a pair of model systems as in this case: the index of directionality should increase if the coupling strength represented by $\epsilon_{1,2}$ in the equations 3.1 is increased. This behavior is clearly seen in Fig. 6.1.
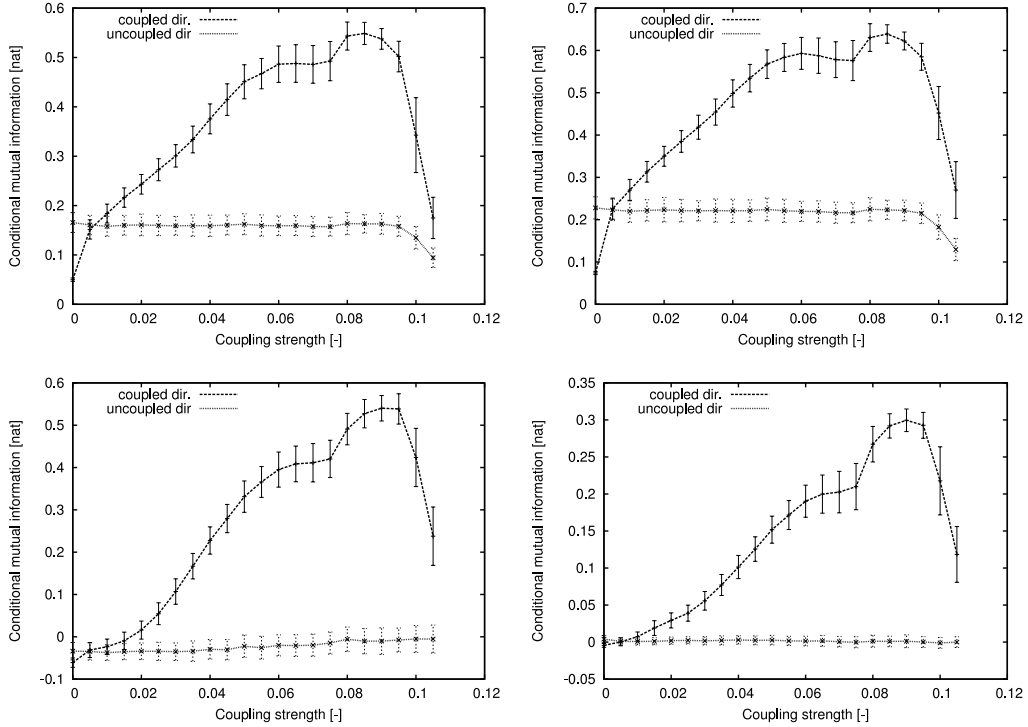
Figure 6.1: Mean conditional mutual information estimates and standard deviations for different estimators: classical histogram with 8 bins (top left), the equiquantal estimator with 8 bins (top right), the k-NN estimator using the 4-th neighbor (bottom left) and using the 16-th neighbor (bottom right). Please note the stability of the reverse direction index for the k-NN method. The length of the supplied time series was 1024 samples.

All the estimators display monotonously increasing values of the CMI index as the coupling strength (ϵ_2 in (3.1)) grows. Around the coupling strength $\epsilon_2 \approx 0.1$ the indices decrease sharply as the systems become synchronized and directionality cannot be reliably estimated anymore. Generalized synchronization sets in at $\epsilon = 0.12$ [23]. There is no clear direction in the flow of information between the systems and this is reflected in the sharp decrease of the CMI index.

6.2 Directionality: Index variability

The observables of the measured processes are random variables and thus each realization of a process as recorded by a time series is different, even under the same set of conditions. For different realizations of the processes, the index of directionality will vary. In this experiment some example distributions will be shown for uncoupled systems and progressively stronger unidirectional coupling on the equiquantal estimator and on the k-NN estimator of conduitional mutual information proposed in this work.

To be able to test the significance of an index obtained from experimental data, where usually only a single time series is available, surrogate testing is applied as described in Chapter 4. Under ideal conditions, the distributions obtained would be identical to those obtained for the ideal surrogates (or equation-based surrogates) described in Chapter 4. We will numerically show how the directionality indices are distributed for permutation surrogates. Moreover, the shape of the distribution is dependent on the strength of coupling, which will be made clear by comparing surrogate histograms from different coupling strengths.

In Fig. 6.2 the (smoothed) histograms for various situations are shown. The left column contains the histograms for the estimates of conditional mutual information from the time series generated from the models (data) the right column contains CMI estimates from permutation surrogates. In each image there are four histograms, for four different values of ϵ_2 (with $\epsilon_1 = 0$ in all cases). Ideally, only the distribution for the CMI index in the direction of coupling computed from the model time series data should react to changing coupling strength. In the other three cases (reverse direction from data, both directions from surrogates), the histograms should not vary with increasing strength of coupling. This ideal behavior is very difficult to reach in practice.

For a positive detection in the direction of coupling, the distributions of CMI indices from data should be located at higher values than the corresponding distributions from surrogates. For a correct rejection in the opposite direction, the histograms should be positioned so that the 95% quantile

of the surrogate distribution is higher than the samples in the distribution
on the data. In this way the hypothesis test will be negative which is the
correct behavior. In Fig. 6.2, it is clearly seen that permutation surrogates
provide surrogate time series from which the estimates in the reverse direc-
tion are slightly higher than those from the model time series (second and
fourth row, compare left and right columns). This is not ideal (sensitivity
may be lower for very small couplings) but neither does this behavior cause
additional false positive detections.
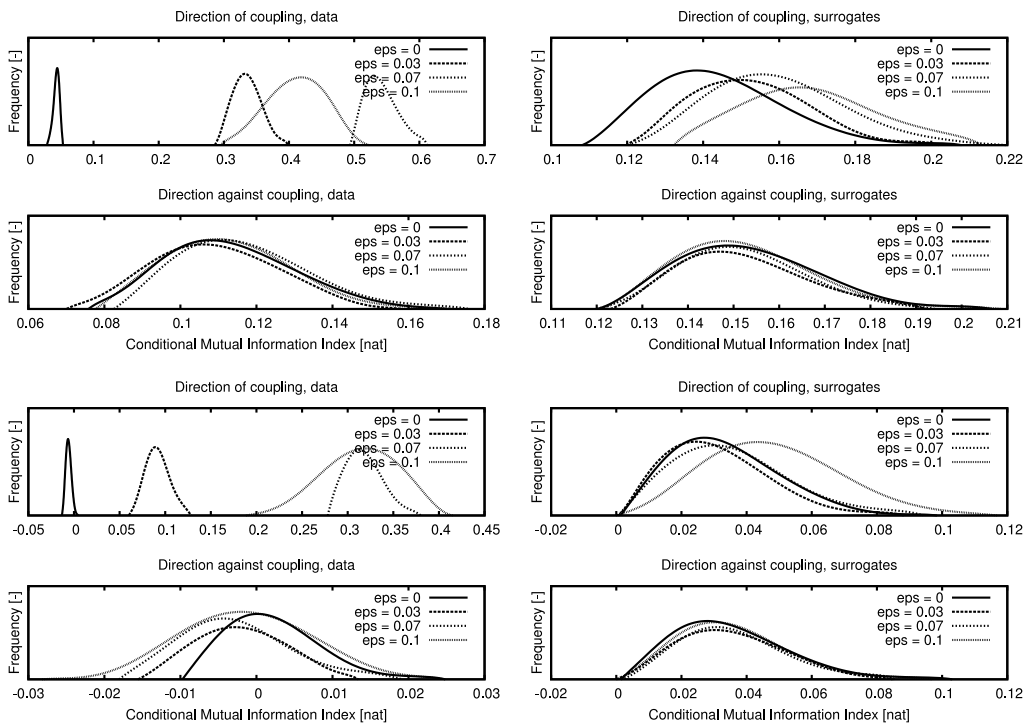
Figure 6.2: Distributions of the conditional mutual information estimates
for selected estimators. Estimates from data (original time series) are on
the left, from permutation surrogates on the right. The top half shows the
results of the equiquantal estimator with 8 bins (upper half) and the bottom
half shows the results of the k-NN estimator using the 16-th neighbor. The
length of the supplied time series was 2048 samples.

6.3 Directionality: Detection statistics

For analysis of experimentally obtained data, the most important aspect of a method is its ability to discriminate between coupled and uncoupled states in either direction. In the following tests, a selection of detection methods is tested on a unidirectionally coupled Rössler 1:1 system. Surrogates were generated using the permutation scheme. The coupling term $\epsilon_1 = 0$ and ϵ_2 was varied between 0 and 0.1. For each coupling, 128 realizations and 128 surrogates were generated. Using the standard hypothesis test described in Chapter 4 at the significance level of 5%, the methods satisfy the requirements of the test if the true positive rate (positive detection if coupling is present in the given direction) is above 95% and the false positive rate (positive detection if there is no coupling in the given direction) is less than 5%. These requirements are not necessarily satisfied for time series which are too short to provide a reliable estimate of the conditional mutual information index.

This experiment shows how selected methods behave depending on the coupling strength and amount of supplied data. In Fig. 6.3 the curves clearly indicate that true positives are increased for weaker couplings when more data is supplied to the method. However false positives also increase. This may be due to the fact that (as has been explained in Chapter 4) permutation surrogates do not preserve long-term correlations that are important in long time series. This causes a lower variance in the estimates of the conditional mutual information index from the surrogates as seen in Fig. 6.4 and the false positive rate rises above the acceptable 5% level. Permutation surrogates are thus adequate for use when shorter time series of less than 400 periods (here 8192 points with the ≈ 20 points per period sampling rate).
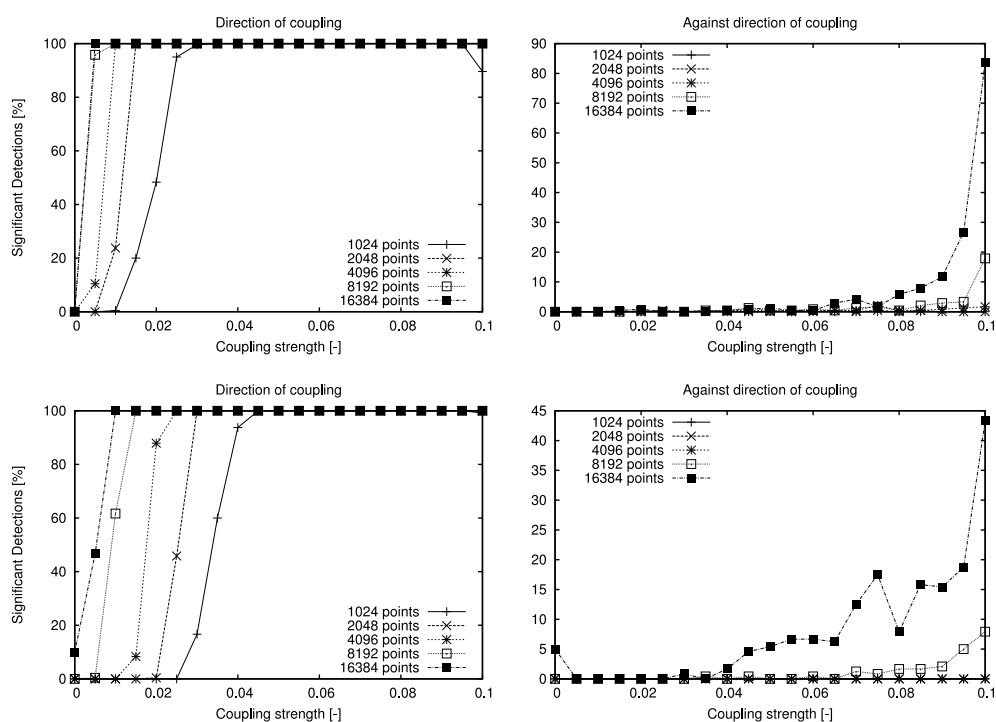
Figure 6.3: Rössler systems 1:1, detection statistics vs. coupling strength for different time series lengths. The equiquantal estimator (8 bins) is on top and the k-NN estimator (16 neighbors) is at the bottom. Left column shows the number of the true positives (positive detections when coupling is present) and the right column shows the number of false positives (positive detections when no coupling is present).
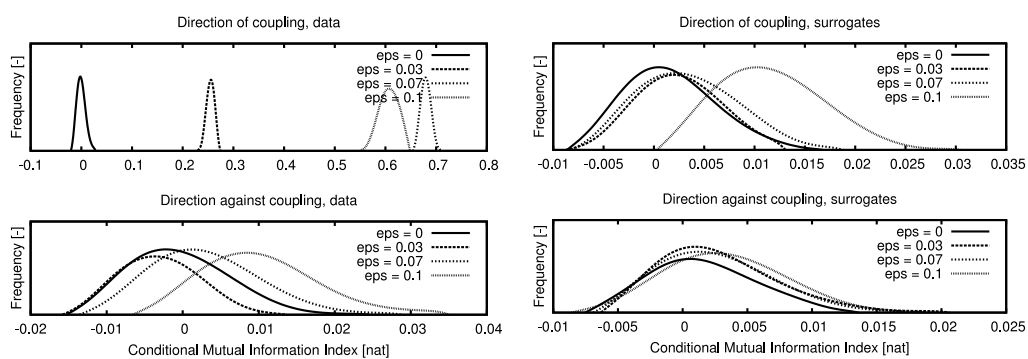
Figure 6.4: Distributions of the CMI index on the data and surrogates in the forward and reverse direction, Rössler systems 1:1. Please note the scale on the horizontal axis indicating that the reverse direction index distribution for the direction against coupling is clearly wider in the model time series (left) than in the surrogate time series (right). The number of samples in the time series is 16384.

6.4 Synchronization: Detection statistics

The established method of detecting phase-synchronized states is using one of the phase indices presented in Chapter 3 with an appropriated surrogate generation method and constructing a hypothesis test in the spirit of Chapter 4. Here we would like to show how this approach fares on model systems where the synchronization threshold is known.

The situation becomes clear if one considers the schematic in Fig. 3.2 depicting a typical transition to synchronization. A correct test for synchronization would classify any pair of systems under given conditions into one of two possible classes { synchronized, unsynchronized }. In the schematic, this corresponds to the grouping { synchronized, dependent or independent }. Any of the surrogates (including the "ideal" model surrogates) described above represent only the null hypothesis of *independent systems*. A hypothesis test based on the above null hypothesis is in fact classifying into the two classes { independent, dependent or synchronized }. However for small amounts of data, the test using standard surrogates has low power and often does not detect weakly dependent systems but detects synchronized systems (this is easier to separate from independent systems because the coupling is stronger) thus conveying the illusion of correctly separating synchronized states from unsynchronized states.

Detailed testing for different amounts of data provided to the algorithms as input clearly shows this effect and moreover shows that as more data is provided to the methods, they converge to a classifier into two states { independent, dependent or synchronized }. This is true for all of the indices listed and all of the surrogates considered. In the following we supply test results from which the convergence behavior becomes clear. We note that ideally, the synchronization test should yield no positive detections for coupling weaker than the threshold ($\epsilon_{1,2} \approx 0.027$) and should detect all cases as synchronized for coupling strengths above the synchronization threshold. Also the efficacy of detection should improve as more data is supplied to the methods.

In Fig. 6.5 the synchronization detection results from the same indices

as in Fig. 3.3 for the same coupling strength range are shown with the null hypothesis distribution generated using Fourier transform surrogates. Please note that the entropy of phase differences has consistently high false positive rates even for independent systems, this indicates that simply estimating the entropy of phase differences may not be sufficient means to separate between even independent and dependent systems. The k-NN mutual information estimator of phase dependence also has a high number of false positives. This is due to the fact that the estimator is based on distances between samples and Fourier transform surrogates significantly affect the distribution of the samples of the time series and thus also the distribution of distances between samples is deformed. An alternate (binning) estimator of mutual information has been tested which does not suffer from this problem. All the plots display the same convergence behavior: as longer time series are made available to the algorithm, systems connected with weaker and weaker coupling are classified as synchronized. This is unsatisfactory as more data should allow for a more precise discrimination between synchronized and unsynchronized states.

In Fig. 6.6 again the same indices have been tested, this time using permutation surrogates. Permutation surrogates cause a very slight deformation in the distribution of distances compared to the Fourier transform surrogates. It is clearly seen from the figure that the distance-based estimator of mutual information has low false positives for both parameter settings (1-st neighbor and 16-th neighbor used to estimate local probability densities). In long time series, the permutation surrogates do not adequately represent the null hypothesis because long-term dependencies are not preserved in the surrogates. Permutation surrogates only preserve the waveform inside a single period and there is no dependency modeling across period boundaries. If the original time series contain long-term dependencies, their destruction causes a bias in the distribution of the index under the null hypothesis and the hypothesis test becomes unbalanced. This is seen for longer time series especially in the k-th nearest neighbor estimator (middle row). Qualitatively, all of the tested indices behave exactly like with Fourier transform surrogates. It is clear that once again, the methods actually discriminate between independent and de-

pendent (or synchronized) states but for short time series, the test has low
power and thus it seems that the methods seem to separate synchronized
states from unsynchronized states.

There are many possible modifications to the above surrogate generation
schemes and an opponent could always state that surrogates used in the above
tests are not sufficiently sophisticated and that better surrogates would yield
different and satisfactory results. This is why the "ideal" equation-based sur-
rogates which represent the theoretical limit of all practical surrogate genera-
tion schemes have been used to test the indices as well. These surrogates are
independent of any surrogate generation algorithm (or modification) because
they are generated directly from the underlying models. Fig. 6.7 summarizes
the results of the test with model based ideal surrogates. Please note that
the horizontal range of coupling strengths $\epsilon_{1,2} \in \langle 0, 0.1 \rangle$ is different from the
above tests ($\epsilon_{1,2} \in \langle 0, 0.04 \rangle$) because the overall sensitivity is smaller. The
qualitative behavior of successively weaker couplings classified as synchro-
nized as longer time series are supplied to the systems is preserved.

The above tests summarize that in practice as well as in theory the cur-
rently applied synchronization detection techniques are not suitable for de-
tecting phase synchronized states. We would like to note here that this
behavior has been found due to large scale testing of indices using computer
clusters. Large scale testing is not standard practice in the community devel-
oping algorithms for testing synchronization and directionality. Publications
in impacted journals do not usually contain plots of detection rates and it is
difficult to understand how effective the proposed methods are.
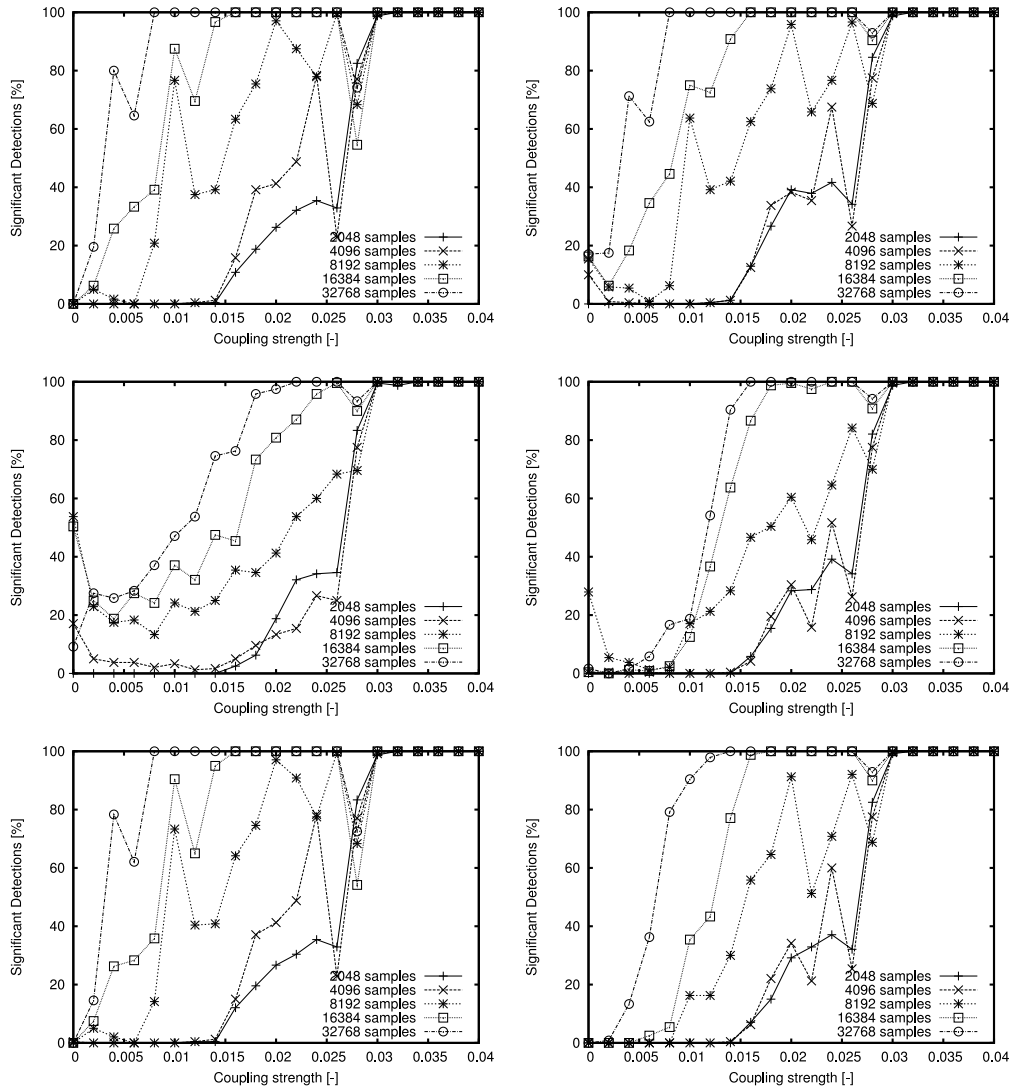
Figure 6.5: Detection rates vs. coupling strength for the symmetrically coupled Rössler pair (3.1) for different amounts of data: conditional probability with 16 bins (top left), entropy of phase differences with 16 bins (top right), Kraskov *et al.*'s estimator of mutual information using 1st neighbor (center left), 16th neighbor (center right), mean phase coherence (bottom left) and binned mutual information (bottom right). The synchronization threshold is at $\epsilon_{1,2} \approx 0.027$. In all of the methods there is a clear tendency to detect weaker and weaker couplings when more data is supplied. The Fourier transform method was applied to generate surrogate time series.
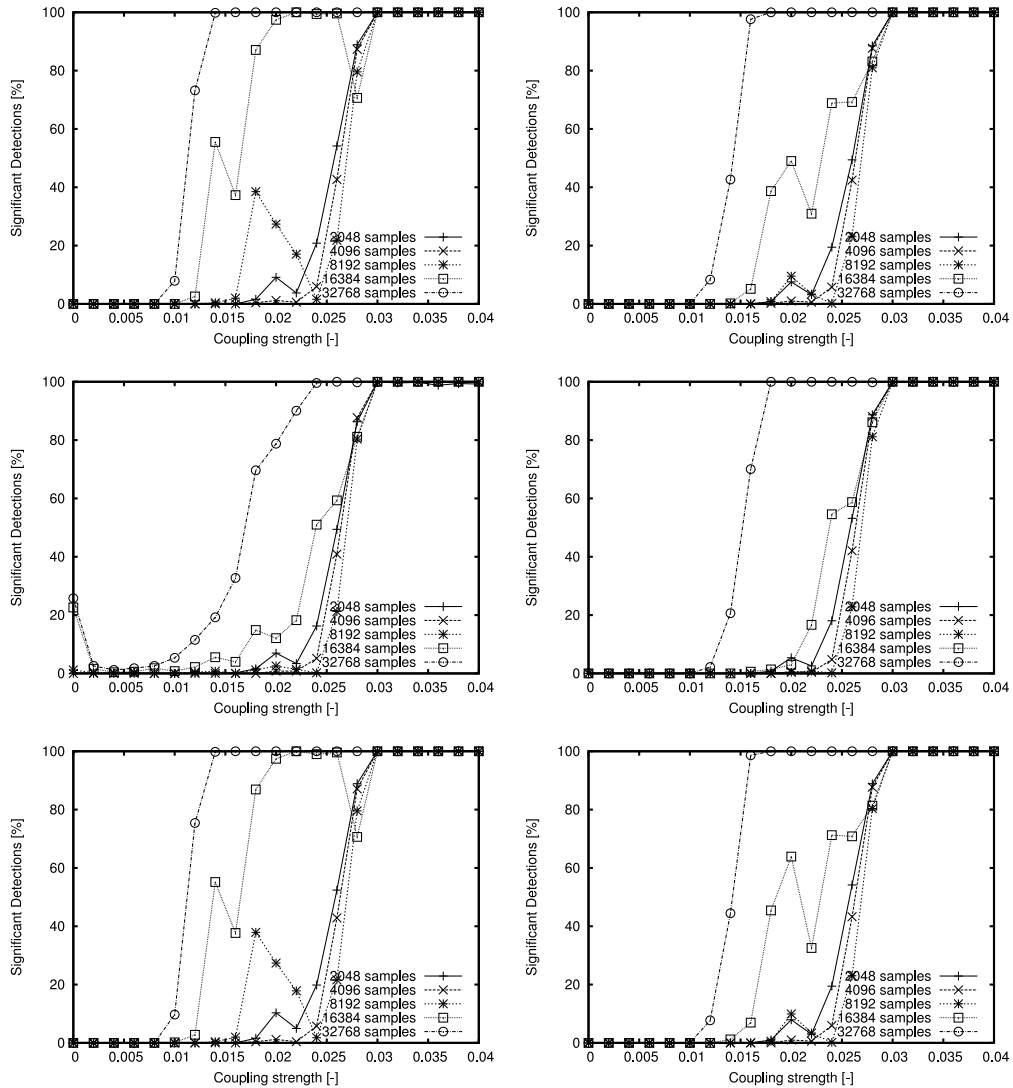
Figure 6.6: Detection rates vs. coupling strength for the symmetrically coupled Rössler pair (3.1) for different amounts of data: conditional probability with 16 bins (top left), entropy of phase differences with 16 bins (top right), Kraskov *et al.*'s estimator of mutual information using 1st neighbor (center left), 16th neighbor (center right), mean phase coherence (bottom left) and binned mutual information (bottom right). The synchronization threshold is at $\epsilon_{1,2} \approx 0.027$. In all of the methods there is a clear tendency to detect weaker and weaker couplings when more data is supplied. The permutation strategy was applied to generate surrogate time series.
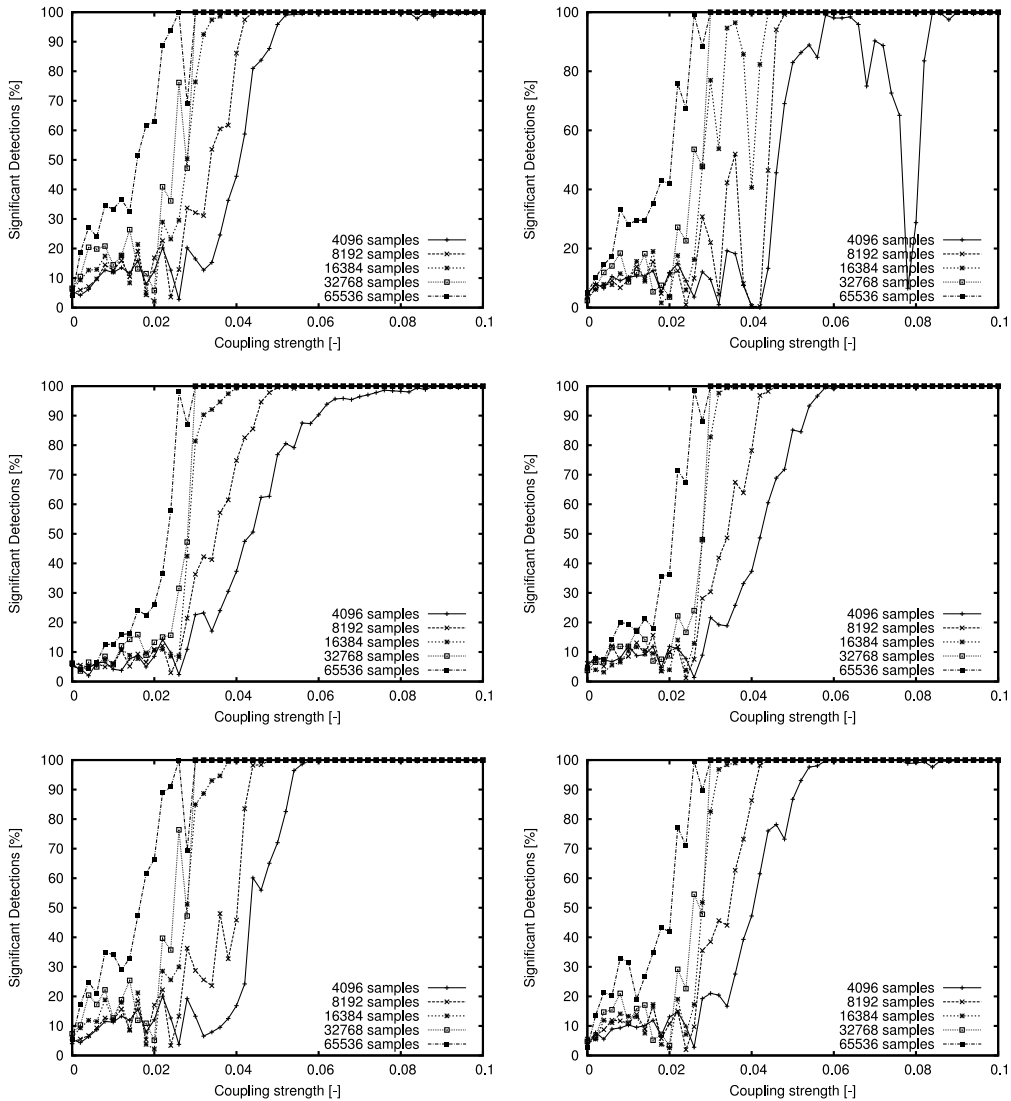
Figure 6.7: Detection rates vs. coupling strength for the symmetrically coupled Rössler pair (3.1) for different amounts of data: conditional probability with 16 bins (top left), entropy of phase differences with 16 bins (top right), Kraskov *et al.*'s estimator of mutual information using 1st neighbor (center left), 16th neighbor (center right), mean phase coherence (bottom left) and binned mutual information (bottom right). The synchronization threshold is at $\epsilon_{1,2} \approx 0.027$. In all of the methods there is a clear tendency to detect weaker and weaker couplings when more data is supplied. The "ideal" model surrogates have been generated to supply the distribution under the null hypothesis. Please note that the horizontal axis range is different from the previous two plot groups.

Chapter 7

Experimental data study

One of the aims of the BRACCIA project is to apply recent findings in the analysis of coupling from time series to data recorded in the waking state and under general anesthesia and to discover factors differentiating between these two states. Methods developed in the framework of non-linear dynamics were applied to experimental data acquired from human volunteers and on an animal model of general anesthesia. The underlying assumption is that the subsystems in the human cardiorespiratory system behave like noisy dynamical systems and can be analyzed as a set of weakly coupled non-linear oscillators. The central problem is then the detection of changes in coupling between respiratory, cardiac and cortical oscillations.

The data from human volunteers was acquired in a clinical setting in the Ulleval Hospital in Oslo and in the Royal Lancaster Infirmary under the supervision of qualified anesthesiologists. The ethical committee had reviewed the procedures and allowed the experiment to proceed. In this study, 25 patients were included (17 from the Ulleval Hospital and 8 from the Lancaster Infirmary).

In this Chapter, interactions between the cardiac and respiratory oscillators are investigated in the data obtained from human volunteers. In the next sections, the full measurement protocol is recounted, the preprocessing procedure is described and the results of the preliminary study involving the cardiac and the respiratory systems are presented.

7.1 Protocol

Measurements were carried out in the waking state and under general anesthesia for spontaneous and controlled respiration depending on the choice of anesthetic for the subject. The aim was to obtain a record of about 20–30 minutes of the activity of the human organism in each state. In this first study only patients with no neurological or degenerative diseases and with no cardiovascular complications were included. Patients that have agreed to provide data to the project were lying still while the recording in the waking state took place. Then general anesthesia was induced using a method which was randomly selected beforehand. One possibility was the use of Sevoflurane (inhalatory anesthetic) together with a muscle relaxant (cisatracurium — trade name Nimbex) after the administration of which the patient was provided with an artificial breathing apparatus. The other possibility is Propofol (short-acting intravenous anesthetic) where no muscle relaxant was administered and the patient continued breathing on his/her own. A total of 10 time series from each patient were measured at a sampling rate of 1024 Hz. For our purposes ECG and the Respiratory signal are most important and will be described in detail.

EEG (electroencephalogram) was measured with 4 channels (EEG1 – EEG4) using BIS (Bispectral index) electrodes. The BIS electrodes are mounted on a strip with 3 electrodes. One of these electrodes is placed near the eye socket and is referenced as the ground electrode. The two remaining electrodes provide a signal that indicates the voltage between themselves and the reference electrode. In analysis the pairs of channels EEG1/2 and EEG3/4 are then again subtracted from each other (i.e. EEG2-EEG1 and EEG4-EEG3) to obtain a "bipolar" montage resulting in two EEG channels available for further processing.

ECG (electrocardiogram) was measured using three electrodes adjusted to obtain well-defined R-peaks: one electrode was placed on the left shoulder, another electrode on the right shoulder and the third electrode was placed

on the lowest rib on the left side of the subject. The ECG signal conditioning channel consists of input protection circuitry, input lowpass filtering, an instrumentation amplifier, a gain amplifier, an active lowpass filter and a reference (virtual ground) driver. The signal is digitized by a 24-bit $\Delta\Sigma$ A/D converter and filtered digitally through LP FIR filter. Finally it is fed through an isolator to the digital part of the system. Input signals are filtered first by lowpass filters: normal mode filter with a cutoff frequency of approximately 3.2kHz and commonmode filter with a cutoff frequency of $\approx$ 50kHz. The filters are implemented to reduce the influence of RF (radio frequency) noise. The ECG signal conditioning channel does not contain a notch filter to eliminate the influence of the mains frequency (50Hz/60Hz) so that the phase integrity of the ECG signal is not compromised.

Blood pressure was measured using a piezoelectric transducer attached to the right first finger.

Respiratory effort was measured using a TSD102 Respiratory effort transducer. It is a piezoelectric sensor which is equipped with a silicon rubber strain assembly to measure the change in the thoracic circumference [91]. An elastic belt was tied around the patients chest and adjusted for optimal data acquisition. This was especially difficult as the inspiration/expiration pattern has changed during general anesthesia and it was important to prevent the belt from being slack or being too tight and exceeding the maximum sensor range of the piezoelectric transducer. The signal conditioning channel of the piezoelectric transducer has an input protection, a transconductance amplifier and an active lowpass filter with cutoff frequency of 16kHz.   Finally the signal is digitized by a 24-bit $\Delta\Sigma$ A/D converter and digitally filtered through a lowpass FIR (finite impulse response) filter with a cutoff frequency 4.9 kHz.

Skin conductivity was measured with two electrodes, the first on the ball of the right thumb, and the other between the first and second joint. Both electrodes were treated with electrical conductivity gel before the attachment.
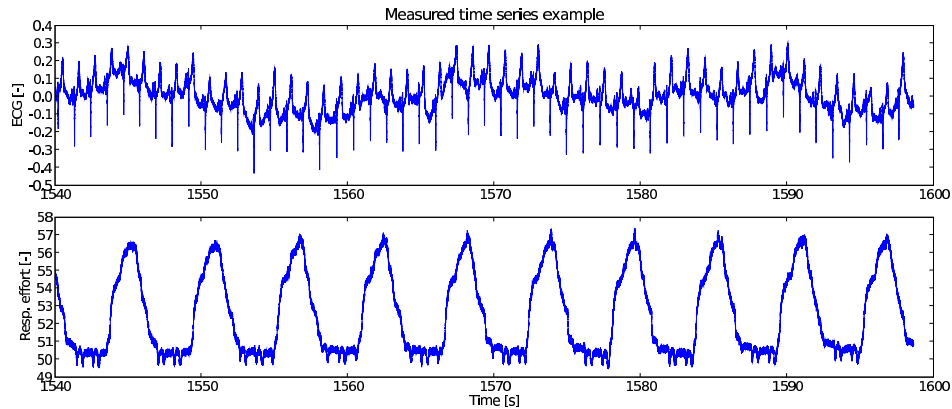
Figure 7.1: Raw time series measured from the patient 118 under general anesthesia.

Temperature was measured with two channels. The first channel originated on an electrode on inside right ankle (medial malleolus) bone, the second channel on inside right wrist (radical styloid) bone. The analog-digital converter was of the $\Delta\Sigma$ type with resolution of 24 bits.

The actual number of effective bits in each sample was of course lower than 24 bits due to effects such as thermal noise and patient motion artifacts.

7.2 Preprocessing

The two time series relevant for further analysis are the ECG and the Respiratory effort time series. Because of the way the respiratory effort was measured (using an elastic belt), the time series contained artefacts in the form of spikes whenever a heartbeat occurred. This effect was created by a mechanical perturbation of the lungs in response to a contraction of the heart muscles. This effect was mitigated by the use of a 1.45s moving average window to smooth the signal. An example of the measured time series is in Fig. 7.1. Phase from the ECG series was extracted by detecting the R-peaks of the signal and linearly interpolating between these events (cf. Sec. 1.3) to obtain marked-events phase. The respiratory effort signal was treated in a similar way - the peaks of the signal were detected and marked. To ensure
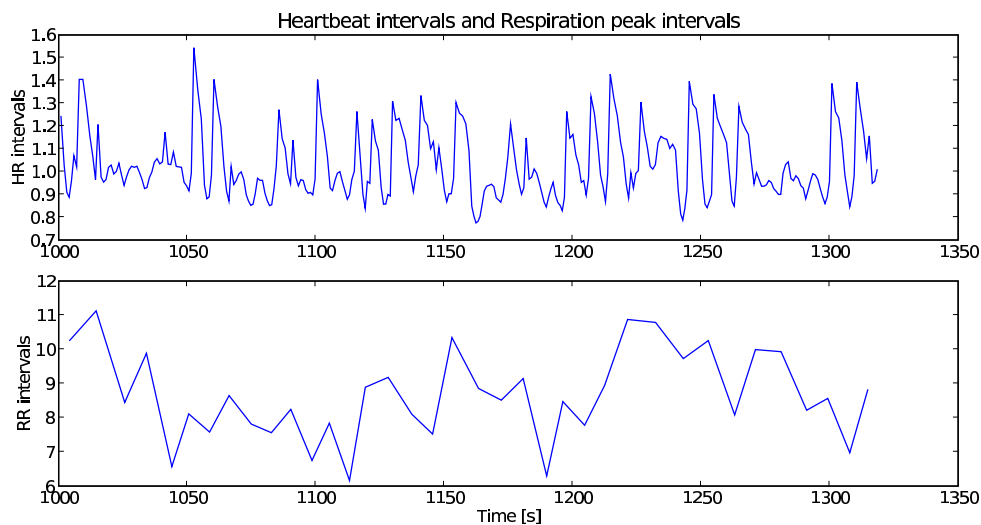
Figure 7.2: The heart rate variability (top) and respiratory rate variability (bottom) for the patient 118 in the waking state (resting).

that local maxima arising from the action of noise (as opposed to those arising from the dynamics) did not contaminate the results, an extra condition was imposed on the peaks - the local maximum must be maximal in some neighborhood (usually about 1/4 of the signal period which was confirmed visually) [1]. Marked-events phase was obtained by interpolating between the obtained event times. In Fig. 7.2, the intervals between successive R peaks of the ECG series (the heart rate variability or HRV) and the intervals between the peaks of the respiratory signal (the respiratory rate variability or RRV) are shown. The HRV and RRV is shown for the same patient under general anesthesia in Fig. 7.3. In this case the breathing became shallower and the heart rate increased. This is however not a general effect.

Finally the series were subsampled by a factor of 40 to obtain approximately 25 samples per period. This ensures that for even for heart rates of 1.3Hz about 20 samples per period are still available. Most patients have their heart rate under this threshold which was selected to balance the amount of samples per period for all patients. Tests on models have previously shown

---

[1]Thanks are due to David Kenwright of the Lancaster University who has performed the above preprocessing procedure
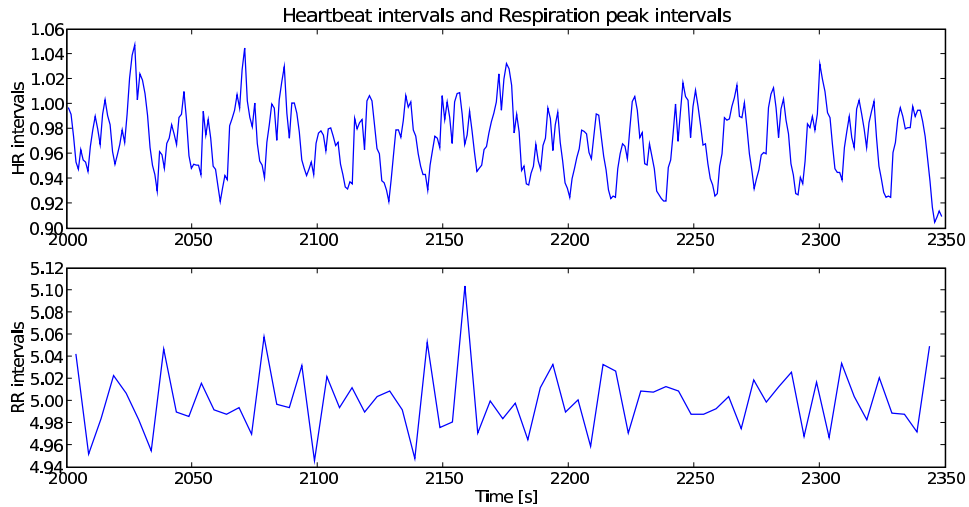
Figure 7.3: The heart rate variability (top) and respiratory rate variability (bottom) for the patient 118 under general anesthesia.

that about 20 points per period are suited for directionality and synchronization analysis using the methods described in this work.

7.3 Analysis

The ECG phase and Respiration phase time series were analyzed using an overlapping moving window strategy with windows of length 8192 points (i.e. about 320s) with 25% overlap (80s). In each window the relevant index was computed and 200 surrogates were generated. The significance of the result was tested in each window independently at the significance level 5% and the resulting indicator was the proportion of significant detections of the index to the total number of windows analyzed in the investigated time series.

This indicator is more stable than using the time course of the index to find regions with higher or lower values of the index as these changes may be brought about by other effects than changing coupling. Such effects can be less noise in the measurements, changed heart rate variability, etc. The indices will of course react to any such dynamical changes with a variation in the resulting value. Another alternative to the selected procedure would

be to test a standardized value for each index

$$K = \frac{i(X) - \overline{i(S)}}{\sigma(i(S))}, \tag{7.1}$$

where $i(X)$ is the value of the index on the data, $\overline{i(S)}$ is the average value of the index on the surrogate data set and $\sigma(i(S))$ is the standard deviation of the index on the surrogate data set. The value K is sometimes identified with the Z-score but this step contains a hidden assumption that the distribution of the index on the surrogates is approximately normal. This index may also give misleading results if the shape of the distribution of the index on the surrogate data set is not stable throughout the entire experiment. The distribution on the surrogate data set is a distribution under the null hypothesis of uncoupled systems and may change independently of the distribution of the index on the actual data set. The above arguments suggest that the proportion of windows with significant results for a given index seems the most robust indicator of changes in the coupling of the cardiorespiratory system given the fact that other changes are expected to occur (e.g. changes in mean frequency of the subsystems).

In the analysis, three indices were computed using a selection of estimators:

- $d_{r \to c}$ average conditional mutual information from the respiratory oscillator to the cardiac oscillator,

- $d_{c \to r}$ average conditional mutual information from the cardiac oscillator to the respiratory oscillator,

- s dependency index between the cardiac and the respiratory oscillators.

The directionality indices $d_{r \to c}$ and $d_{c \to r}$ were computed with three different methods to test if the results largely depend on the method:

- k-NN, the k-nearest neighbor estimator suggested in this work (Sec. 5),

- CINT, the cross-redundancy estimator using the correlation integral (Sec. 2.2.2),

- EQQ, the equiquantal estimator (Sec. 2.2.1).

The motivation behind applying different methods is to examine how the results of the analysis are affected by concentrating on different features of the signal (e.g. distances between samples — k-NN and CINT, relationships between discretized series - EQQ) when computing the same functional: conditional mutual information. The absolute values of the proportion of significant values are expected to vary but all the methods should react in a consistent manner to the state of consciousness of the subject (waking or under general anesthesia) if the effect of the change of state is stable.

Multiple dependency indices s were also considered

- CPR, the conditional probability (Sec. 3.2.1),

- k-NN, mutual information estimated using the method of Kraskov *et al.* (Sec. 3.2.3),

- QNT, mutual information estimated using the equiquantal approach (Sec. 3.2.3).

It is known that dependency of the cardiac and respiratory subsystems increases during anesthesia [76]. It is expected that the present analysis will be consistent with these results. The computational results summarized in Figs. 3.3, 6.5, 6.6 clearly indicate that each method of computing the statistical dependency between signals gives quite different results for a wide set of coupling strengths from non-existent couplings to a phase-synchronized state. Here we investigate what sort of variability will there be between the methods on a real dataset. Usually in experimental works, investigators only use one method of quantifying the dependence or directionality and then the variability with respect to the method used is not immediately apparent.

7.4   Results

The dependence indices paint a consistent picture of what is happening within the cardiorespiratory system: all of the presented indices increase

when the patient is in the anesthetized state. The absolute values of the indices are quite different and are sensitive to the choice of parameters (Fig. 7.4 for the k-NN estimator $k = 32$ and $k = 8$). Please note that the k-NN index is biased negatively on short time series for large k parameters and that is why the index acquires negative values in some cases. This does not affect the surrogate test because the estimators have identical bias on the surrogates. The distributions of the significant results compared all results are slightly different across methods, however the median values of the distributions are very similar across all methods and parameters (not all analyzed methods shown here). The shift between the distributions is also consistent across all analysis methods — clearly in the anesthetized state, the proportion of significant detections grows considerably (to approximately twice the amount of the significant detections in the waking state). The k-NN estimator with $k = 32$ neighbors even exhibits an opposite change of the magnitude of the index itself (cf. top right image in Fig. 7.4) but the results of the surrogate tests is again in agreement with the rest of the methods.

No compensation has been done for the different frequencies of the two systems and therefore the mean phase coherence method was not used in the analysis as it requires that the frequency ratio is taken into account in the generalized phase difference. Since the ratio of frequencies is not stable during the measurement of a single patient this might introduce difficulties as the ratio would have to be adjusted in each analysis window. This may compromise the consistency of the measurements. Since methods based on mutual information and on conditional probability do not require such corrections unless they are applied in the regime of small sample sizes, they may be easier to use in practice.

The analysis of directionality reveals another clear effect of general anesthesia on the cardiorespiratory system: the directional influence from the lungs to the heart is reduced and the opposite influence is increased. This is consistent with a shift in directionality in the cardiorespiratory system. In the waking state, directional influence is usually present from the lungs towards the heart, so called "Respiratory sinus arrhythmia" or variation of the heart rate according to the inspiration/expiration cycle of the lungs. This
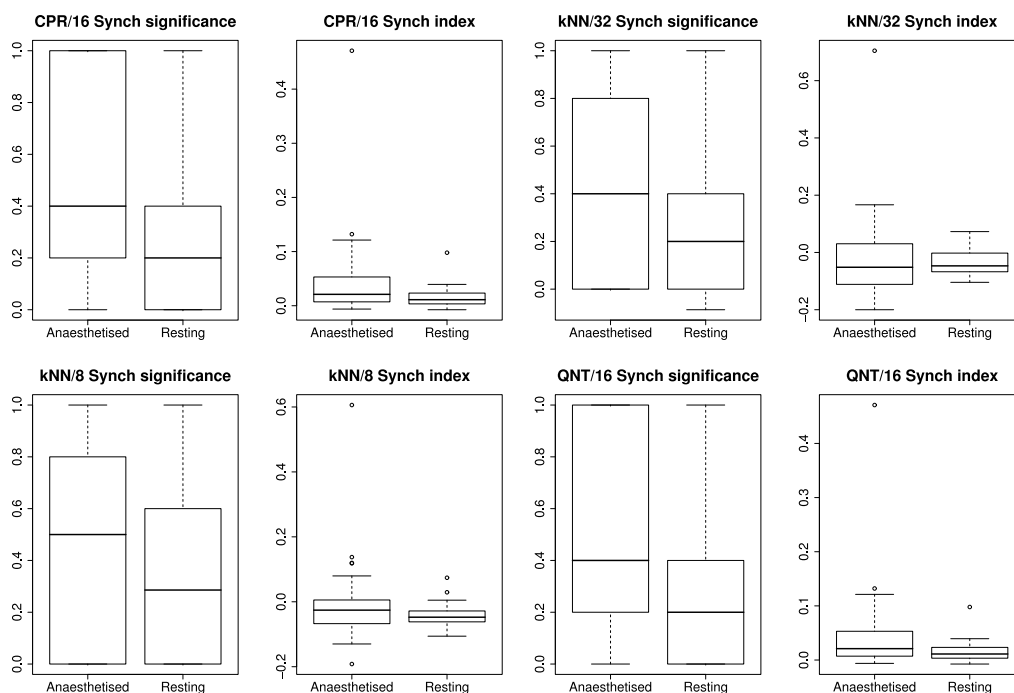
Figure 7.4: Box plots (distribution summaries) for selected dependence indices: conditional probability CPR with 16 bins (top left), k-nearest neighbors k-NN with 32 neighbors (top right), the same with 8 neighbors (bottom left) and mutual information QNT estimated using the equiquantal estimator with 16 bins (bottom right).

fact is consistent with the summary in Fig. 7.5, where the box plots show that in the waking state, the proportion of significant directionality results is well above 60% for all methods. Under general anesthesia, this influence is greatly reduced. On the other hand, directional influence from the heart to the lungs is not clear in the waking state but the detected significant results are much higher in the anesthetized state for all methods and parameters with the exception of the CINT/0.3 method (Cross-redundancy, $\epsilon = 0.3$). Cross-redundancy methods use a fixed-volume approach to estimating the local PDFs of the time series and do not adapt to data like, for example the k-NN method which adjusts the size of the neighborhood to the local density. An inadequate neighborhood size may be the reason that cross-redundancy does not behave the same for different parameters ϵ.

Observing the results from different methods and parameter settings, it is clear that there is some variation between the methods and even with respect to the parameters within one method. The medians of the distribution (indicated by a thick line in Fig. 7.5) are however very stable across parameter choices and even across different methods. There is also a clear agreement between the methods in the change of the indicator between general anesthesia and the waking state for both directionalities.
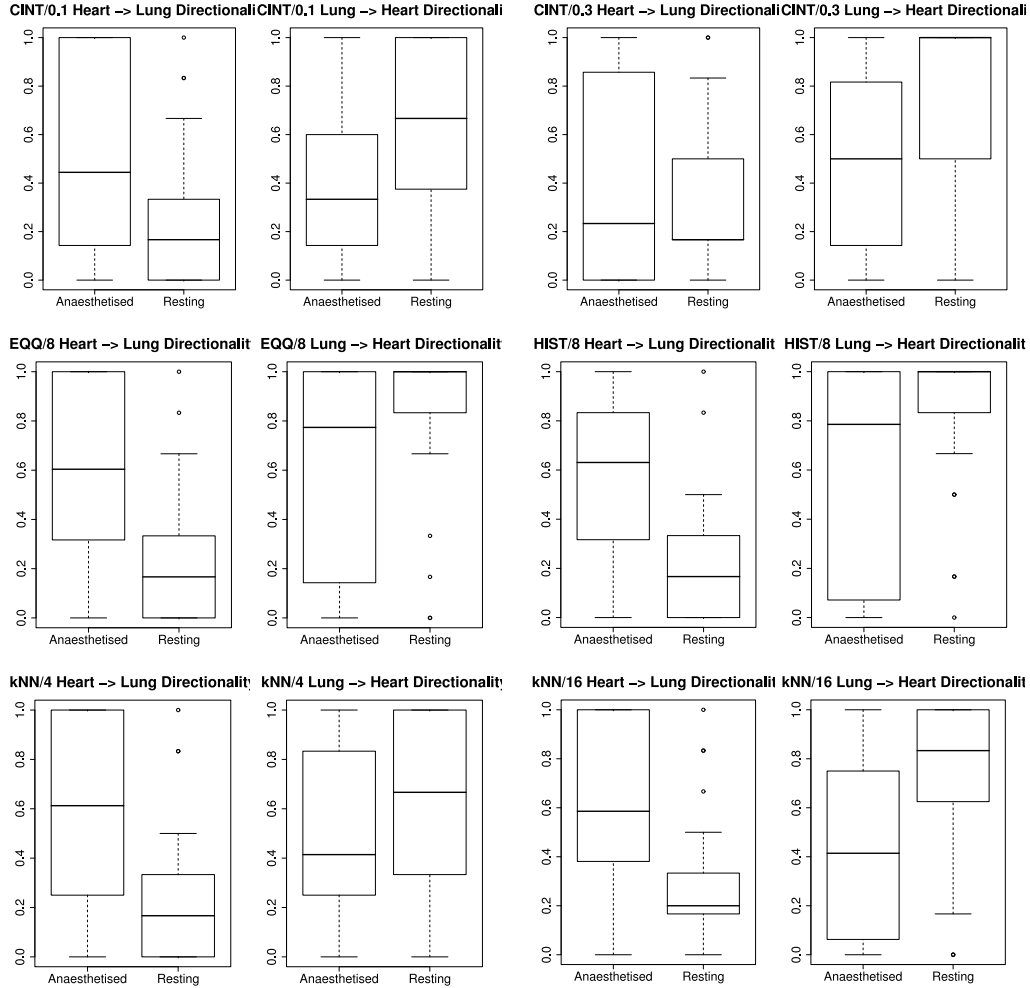
Figure 7.5: Summary of the results from the analysis of directional influence obtained from the preliminary BRACCIA dataset. Each method has different distributions of the computed metric (proportion of significant results) but the methods agree on the median of the distribution and on the effect that general anesthesia has on the cardiorespiratory system interactions: the directional influence from the lungs to the heart is decreased and the directional influence from the heart to the lungs is increased. Estimators: cross-redundancy with $\epsilon = 0.1$ (top left), the same with $\epsilon = 0.3$ (top right), equiquantal estimator with 8 bins (middle row left), simple histogram estimator with 8 bins (middle row right), k-nearest neighbors estimator with 4 neighbors (bottom left) and the same with 16 neighbors (bottom right).

Chapter 8

Conclusion

In this work the framework for analyzing systems of self-sustained non-linear oscillators was presented and the necessary concepts were introduced. The conditions for the application of the phase dynamics approach and it's advantages were described. The concept of weak interactions was presented and the problem of quantification of weak interactions was divided into two classes: synchronization detection and directionality analysis.

The core problem studied in this work is the problem of analyzing the full range of weak interactions in a pair of non-linear oscillators. The effect of coupling strength on synchronization properties was investigated and numerical experiments showing how synchronized states can be detected in the paradigmatic pair of Rössler oscillators were performed. Methods of quantifying strength of directional coupling have been introduced and information-theoretic methods have been studied in detail. Conditional mutual information was introduced and explained as the functional of choice for estimating the "net flow of information" [41]. Selected estimation procedures based on different concepts were theoretically investigated and numerically tested and their behavior depending on their free parameter (if any) was analyzed. A new estimator based on [70, 71] converging to the true value of conditional mutual information independently of the value of its free parameter has been derived. The estimator has been empirically shown to have the properties that have been theoretically expected. Although the estimator has favorable

81

properties, caution is advised when applying the estimator to real data as noise and deformations of the measured signal can perturb the metric relationships in the sample space. Binning estimators seem to be less sensitive to the influence of measurement noise and signal deformations.

The current methodology for detecting phase synchronization was analyzed and it was ascertained that frequently applied methods detect phase synchronization in the weaker sense. This means that the tendency to synchronize is detected rather than phase-synchronized states. The currently employed methods results in marking any dependent states as synchronized even if the coupling is not strong enough to actually cause the systems to enter a phase-synchronized state. Large scale testing was conducted to verify this phenomenon for a selection of frequently applied methods. A new approach to detecting synchronized states using the null hypothesis of the phase-synchronized state was introduced and shown to detect phase-synchronized states satisfactorily. The effectiveness of the detector was again shown using detailed numerical studies.

The bias and variance of the estimators of conditional mutual information have been investigated for a pair of unidirectionally linearly coupled ARMA (Autoregressive, Moving Average) processes, where the conditional mutual information can be estimated analytically from the correlation matrix. Since it is not in general possible to use the absolute values of the directionality indices to analyze experimental data, the significance of an obtained directionality index value must be verified using a hypothesis test. The method of surrogate data was introduced as a possible solution to this problem. Various methods of generating surrogate data with different properties have been recounted. Numerical experiments using a pair of similar Rössler systems have been performed to analyze the efficacy of various estimators with respect to the permutation surrogate generation method.

A selection of dependence analysis methods and directionality detection methods were applied to electrocardiogram and respiratory effort time series obtained within the project BRACCIA. Time series originating from 25 patients were analyzed with the goal of finding differences in the functioning of the cardiorespiratory system between the waking state and under general

anesthesia. Previous findings on stronger overall coupling between the two subsystems were confirmed by the present analysis. It was found that in the preliminary study there were clear changes of directional influence: in the waking state, the respiratory system affected the cardiac oscillator more than under general anesthesia and vice-versa for the influence of the cardiac system on the respiratory system. The indication of directional influence was stable even when the free parameter of some methods was changed to test the stability of the results.

Further work will concentrate on generalizing the above framework to a system of many coupled oscillators instead of studying the reduced situation of a single pair of systems. This situation arises for example when measuring the activity of the human brain. If for example magnetic resonance imaging (MRI) is used to obtain a multivariate signal from the brain, the resulting data contains tens of thousands of time series, with each characterizing brain activity at a high spatial resolution using a BOLD (blood oxygen level dependent) signal. Another avenue of research consists in trying to derive an index capturing directional influence between systems that would be robust with respect to deformations of the time series which are theoretically difficult to analyze. Enormously helpful in practice would be an algorithm that would include an internal significance test thus eliminating the need for a separate surrogate generation algorithm.

Bibliography

[1] M. G. Rosenblum, A. S. Pikovsky, and J. Kurths. Phase Synchronization of Chaotic Oscillators. *Physical Review Letters*, 76(11):1804–1807, 1996.

[2] A. Pikovsky, M. Rosenblum, and J. Kurths. *Synchronization. A Universal Concept in Nonlinear Sciences*. Cambridge University Press, Cambridge, 2001.

[3] C. Schäfer, M.G. Rosenblum, J. Kurths, and H.-H. Abel. Heartbeat synchronization with ventilation. *Nature*, 392, 1998.

[4] M. Paluš. Nonlinear Dynamics in the EEG Analysis: Disappointments and Perspectives. In N. Pradhan, P.E. Rapp, and R. Sreenivasan, editors, *Nonlinear Dynamics and Brain Functioning*, pages 201–216, New York, USA, 1999. Nova Science Publishers.

[5] C. Allefeld, A. Müller, and J. Kurths. Eigenvalue decomposition as a generalized Synchronization Cluster Analysis. *International Journal of Bifurcation and Chaos*, 17:3493–3497, 2007.

[6] D. Maraun and J. Kurths. Epochs of phase coherence between El Niño/Southern Oscillation and Indian monsoon. *Geophysical Research Letters*, 32(15), 2005.

[7] M. Paluš and D. Novotná. Quasi-biennial oscillations extracted from the monthly NAO index and temperature records are phase-synchronized. *Nonlinear Processes in Geophysics*, 13:287–296, 2006.

[8] F. Takens. Detecting strange attractors in turbulence. In D.A. Rand and L.S. Young, editors, *Dynamical systems and turbulence*, volume 898, pages 366–381, Berlin, 1981. Springer.

[9] T. Sauer, J. A. Yorke, and M. Casdagli. Embedology. *Journal of Statistical Physics*, 65(3–4):579–616, 1991.

[10] T. Sauer. Reconstruction of dynamical systems from interspike intervals. *Physical Review Letters*, 72(24):3811–3814, 1994.

[11] D. Gabor. Theory of communication. *J. IEE London*, 93:429–457, 1946.

[12] M. Le Van Quyen, J. Foucher, J-P. Lachaux, E. Rodriguez, A. Lutz, J. Martinerie, and F. J. Varela. Comparison of Hilbert transform and wavelet methods for the analysis of neuronal synchrony. *J. Neurosci. Meth.*, 111:83–98, 2001.

[13] F. Mormann, K. Lehnertz, P. David, and C. E. Elger. Mean phase coherence as a measure for phase synchronization and its application to the EEG of epilepsy patients. *Physica D*, 144:358–369, 2000.

[14] Christiaan Huygens. *Horologium Oscillatorium, sive de motu pendulorum*. Apud F. Muguet, Paris, 1673.

[15] D.A. Smirnov and R.G. Andrzejak. Detection of weak directional coupling: Phase-dynamics approach versus state-space approach. *Physical Review E*, 71:036207, 2005.

[16] V.N. Smelyanskiy, D.G. Luchinsky, A. Stefanovska, and P.V.E. McClintock. Inference of a Nonlinear Stochastic Model of the Cardiorespiratory Interaction. *Physical Review Letters*, 94:098101, 2005.

[17] D.A. Smirnov, M.B. Bodrov, J.L. Perez Velazquez, R.A. Wennberg, and B.P. Bezruchko. Estimation of coupling between oscillators from short time series via phase dynamics modeling: Limitations and application to EEG data. *Chaos*, 15:024102, 2005.

[18] M. Paluš and D. Hoyer. Detecting nonlinearity and phase synchronization with surrogate data. *IEEE Engineering in Medicine and Biology*, 17(6), 1998.

[19] M. Bračič Lotrič and A. Stefanovska. Synchronization and modulation in the human cardio-respiratory system. *Physica A*, 283(3–4), 2000.

[20] S.J. Schiff, P. So, T. Chang, R.E. Burke, and T. Sauer. Detecting dynamical interdependence and generalized synchrony through mutual prediction in a neural ensemble. *Physical Review E*, 54:6708–6724, 1996.

[21] M. Le Van Quyen, J. Martinerie, C. Adam, and F.J. Varela. Nonlinear analyses of interictal EEG map the brain interdependences in human focal epilepsy. *Physica D*, 127, 1999.

[22] P. Tass, M.G. Rosenblum, J. Weule, J. Kurths, A.S. Pikovsky, J. Volkmann, A. Schnitzler, and H.-J. Freund. Detection of n:m Phase Locking from Noisy Data: Application to Magnetoencephalography. *Physical Review Letters*, 81, 1998.

[23] M. Paluš, V. Komárek, Z. Hrnčíř, and K. Štěrbová. Synchronization as adjustment of information rates: Detection from bivariate time series. *Physical Review E*, 63, 2001.

[24] U. Parlitz, L. Junge, W. Lauterborn, and L. Kocarev. Experimental observation of phase synchronization. *Physical Review E*, 54(2), 1996.

[25] N.F. Rulkov, K.M. Sushchik, L.S. Tsimring, and H.D.I. Abarbanel. Generalized synchronization of chaos in directionally coupled chaotic systems. *Physical Review E*, 51, 1995.

[26] L. Kocarev and U. Parlitz. Synchronizing Spatiotemporal Chaos in Coupled Nonlinear Oscillators. *Physical Review Letters*, 76, 1996.

[27] E. N. Lorenz. Deterministic Nonperiodic Flow. *Journal of the Atmospheric Sciences*, 20:130–141, 1963.

[28] P. Grassberger and I. Procaccia. Measuring the strangeness of strange attractors. *Physica D: Nonlinear Phenomena*, 9(1–2):189–208, 1983.

[29] O. E. Rössler. An Equation for Continuous Chaos. *Physics Letters A*, 57:397–398, 1976.

[30] H. Froehling, J. P. Crutchfield, D. Farmer, N. H. Packard, and R. Shaw. On Determining the dimension of chaotic flows. *Physica D*, 3:605–617, 1981.

[31] G. V. Osipov, B. Hu, Ch. Zhou, M. V. Ivanchenko, and J. Kurths. Three Types of Transitions to Phase Synchronization in Coupled Chaotic Oscillators. *Physical Review Letters*, 91(2):024101, Jul 2003.

[32] T. Schreiber and A. Schmitz. Improved surrogate data for nonlinearity tests. *Physical Review Letters*, 77:635–638, 1996.

[33] J. Theiler, S. Eubank, A. Longtin, B. Galdrikian, and J.D. Farmer. Testing for nonlinearity in time series: The method of surrogate data. *Physica D*, 58:77–94, 1992.

[34] C. W. J. Granger. Investigating causal relations by econometric models and cross-spectral methods. *Econometrica*, 37:424–438, 1969.

[35] H. Kantz and T. Schreiber. *Nonlinear time series analysis*. Cambridge University Press, New York, NY, USA, 1997.

[36] J. Arnhold, P. Grassberger, K. Lehnertz, and C. E. Elger. A robust method for detecting interdependences: application to intracranially recorded EEG. *Physica D*, 134:419–430, 1999.

[37] R. Quian Quiroga, J. Arnhold, and P. Grassberger. Learning driver-response relationships from synchronization patterns. *Physical Review E*, 61:5142–5148, 2000.

[38] M.G. Rosenblum and A.S. Pikovsky. Detecting direction of coupling in interacting oscillators. *Physical Review E*, 64:045202, 2001.

[39] D.A. Smirnov and B.P. Bezruchko. Estimation of interaction strength and direction from short and noisy time series. *Physical Review E*, 68:046209, 2003.

[40] T. Schreiber. Measuring information transfer. *Physical Review Letters*, 85:461–464, 2000.

[41] M. Paluš and A. Stefanovska. Direction of coupling from phases of interacting oscillators : An information-theoretic approach. *Physical Review E*, 67, 2003.

[42] K. Schindler-Hlaváčková, M. Paluš, M. Vejmelka, and J. Bhattacharya. Causality detection based on information-theoretic approaches in time series analysis. *Physics Reports*, 441:1–46, 2007.

[43] T.M. Cover and J.A. Thomas. *Elements of information theory*. Wiley-Interscience, New York, NY, USA, 1991.

[44] M. Paluš and M. Vejmelka. Directionality of coupling from bivariate time series: How to avoid false causalities and missed connections. *Physical Review E*, 75:056211, 2007.

[45] R. Moddemeijer. On estimation of entropy and mutual information of continuous distributions. *Signal Processing*, 16(3):233–248, 1989.

[46] A.M. Fraser and H.L. Swinney. Independent coordinates for strange attractors from mutual information. *Physical Review A*, 33(2):1134–1140, 1986.

[47] G.A. Darbellay and I. Vajda. Estimation of the information by an adaptive partitioning of the observation space. *Information Theory, IEEE Transactions on*, 45:1315–1321, 1999.

[48] G.A. Darbellay. An estimator of the mutual information based on a criterion for conditional independence. *Computational Statistics and Data Analysis*, 32:1–17, 1999.

[49] G. A. Darbellay and I. Vajda. Entropy expressions for multivariate continuous distributions. *IEEE Trans. Inf. Theory*, 46(2):709–712, 2000.

[50] R.L. Dobrushin. General formulation of Shannon's main theorem in information theory. *Transactions of the American Mathematical Society*, 33:323–438, 1959.

[51] A. Renyi. On measures of entropy and information. In *4th Berkeley Symposium on Mathematical Statistics and Probability*, volume 1, pages 547–561, 1961.

[52] B. Pompe. Ranking and Entropy Estimation in Nonlinear Time Series Analysis. In H. Kantz, J. Kurths, and G. Mayer-Kress, editors, *Nonlinear Analysis of Physiological Data*, Berlin, 1998. Springer.

[53] C. De Boor. *A Practical Guide to Splines*. Springer, Berlin, 1978.

[54] C. O. Daub, R. Steuer, J. Selbig, and S. Kloska. Estimating mutual information using B-spline functions — an improved similarity measure for analysing gene expression data. *BMC Bioinformatics*, 5, 2004.

[55] D. Prichard and J. Theiler. Generalized redundancies for time series analysis. *Physica D*, 84:476–493, 1995.

[56] R. Savit and M. Green. Time series and dependent variables. *Physica D: Nonlinear Phenomena*, 50(1):95–116, 1991.

[57] Y.I. Moon, B. Rajagopalan, and U. Lall. Estimation of mutual information using kernel density estimators. *Physical Review E*, 52(3):2318–2321, 1995.

[58] R. Steuer, J. Kurths, C.O. Daub, J. Weise, and J. Selbig. The mutual information: Detecting and evaluating dependencies between variables. *Bioinformatics*, 18:231–240, 2002.

[59] B.W. Silverman. *Density Estimation for Statistics and Data Analysis*. Chapman & Hall/CRC, London, 1986.

[60] J.A. Barnes, H.H. Sargent, and P.V. Tryon. Sunspot cycle simulation using random noise. In R.O. Pepin, J.A. Eddy, and R.B. Merrill, editors, *The Ancient Sun*, pages 159–163, New York, 1980. Pergamon Press.

[61] M. Paluš. Testing for nonlinearity using redundancies: Quantitative and qualitative aspects. *Physica D*, 80:186–205, 1995.

[62] S. Bocaletti, J. Kurths, G. Osipov, D.L. Valladares, and C.S. Zhou. The synchronization of chaotic systems. *Physics Reports*, 366:1–101, 2002.

[63] M.S. Baptista, T. Pereira, and J. Kurths. Upper bounds in phase synchronous weak coherent chaotic attractors. *Physica D*, 216:260–268, 2006.

[64] M. Hoke, K. Lehnertz, C. Pantev, and B. Lütkenhöner. Spatiotemporal aspects of synergetic processes in the auditory cortex as revealed by the magnetoencephalogram. In E. Basar and Th. Bullock, editors, *Dynamics of cognitive and sensory processing in the brain*, pages 84–105, Berlin, Heidelberg, New York, 1988. Springer.

[65] M. Paluš. Detecting nonlinearity in multivariate time series. *Physics Letters A*, 213:138–147, 1996.

[66] Y. Kuramoto. *Chemical Oscillations, Waves and Turbulence*. Springer, Berlin, 1984.

[67] K.V. Mardia. *Probability and Mathematical Statistics: Statistics of Directional Data*. Academic Press, London, 1972.

[68] C. Allefeld and J. Kurths. Testing for phase synchronisation. *Int. J. Bif. Chaos*, 14(2):406–416, 2004.

[69] C. Shannon. A Mathematical Theory of Communication. *The Bell System Technical Journal*, 27(3):379–423, 1948.

[70] A. Kraskov, H. Stoegbauer, and P. Grassberger. Estimating Mutual Information. *Physical Review E*, 69, 2004.

[71] L. F. Kozachenko and N. N. Leonenko. Sample estimate of the entropy of a random vector. *Probl. Inf. Trans.*, 23:9–16, 1987.

[72] A. S. Pikovsky, M. G. Rosenblum, and J. Kurths. Synchronization in a Population of Globally Coupled Chaotic Oscillators. *Europhysics Letters*, 34(3):165–170, 1996.

[73] M. Thiel, M.C. Romano, J. Kurths, M. Rolfs, and R. Kliegl. Twin surrogates to test for complex synchronisation. *Europhysics Letters*, 75:535–541, 2006.

[74] J. Neyman and E. S. Pearson. On the Problem of the Most Efficient Tests of Statistical Hypotheses. *Philosophical Transactions of the Royal Society*, 231:289–337, 1933.

[75] James W. Cooley and John W. Tukey. An algorithm for the machine calculation of complex Fourier series. *Mathematical Computations*, 19:297–301, 1965.

[76] A. Stefanovska, H. Haken, P. V. E. McClintock, M. Hožič, F. Bajrovič, and S. Ribarič. Reversible Transitions between Synchronization States of the Cardiorespiratory System. *Physical Review Letters*, 85:4831–4834, 2000.

[77] B. Musizza, A. Stefanovska, P. V. E. McClintock, M. Paluš, J. Petrovcic, S. Ribaric, and F. F. Bajrovič. Interactions between cardiac, respiratory, and EEG-delta oscillations in rats during anaesthesia. *Journal of Physiology*, 580:315–326, 2007.

[78] N. Marwan, M.C. Romano, M Thiel, and J. Kurths. Recurrence Plots for the Analysis of Complex Systems. *Physics Reports*, 438:237–329, 2007.

[79] J. P. Eckmann, S. O. Kamphorst, and D. Ruelle. Recurrence Plots of Dynamical Systems. *Europhysics Letters*, 5:973–977, 1987.

[80] M.N. Goria, N.N. Leonenko, V.V. Mergel, and P.L. Novi Inverardi. A new class of random vector entropy estimators and its applications in testing statistical hypothese. *Nonparametric Statistics*, 17:277–297, 2005.

[81] P. Grassberger. Generalizations of the Hausdorff dimension of fractal measures. *Physics Letters A*, 107(3):101–105, 1985.

[82] R.L. Somorjai. Methods for Estimating the Intrinsic Dimensionality of High-Dimensional Point Sets. In G. Mayer-Kress, editor, *Dimensions and Entropies in Chaotic Systems*, Berlin, 1986. Springer.

[83] J. L. Bentley. Multidimensional binary search trees used for associative searching. *Communications of the ACM*, 18:509–517, 1975.

[84] P. Grassberger. An optimized box-assisted algorithm for fractal dimensions. *Physics Letters A*, 148:63–68, 1990.

[85] M. Vejmelka and K. Hlaváčková-Schindler. Estimation in Higher Dimensions: A Speed-Up of a k-Nearest Neighbor Based Estimator. In *Adaptive and Natural Computing Algorithms*, volume 4431, pages 790–797, Berlin, 2007. Springer.

[86] W. H. Press, S. A Teukolsky, W. T. Vetterling, and B. P. Flannery. *Numerical Recipes*. Cambridge University Press, Cambridge, 1992.

[87] P. R. Bevington and D. K. Robinson. *Data Reduction and Error Analysis for the Physical Sciences*. McGraw-Hill, New York, 1992.

[88] R. von Mises. *Mathematical Theory of Probability and Statistics*. Academic Press, New York, 1964.

[89] P. J. Huber. *Robust statistics*. Wiley, New York, 1981.

[90] L. R. Launer and G. N. Wilkinson. *Robustness in statistics*. Academic Press, New York, 1979.

[91] J. Petrovcic, B. Musizza, and A. Svetek. Cardio&Brain Signals: User Manual. Technical report, Jozef Stefan Institute, Ljubljana, Slovenia, 2008.